

When does a Fermi puddle become a Fermi sea? Emergence of Pairing in Two-Dimensional Trapped Mesoscopic Fermi Gases

Emma Laird^{1,*}, Brendan Mulkerin², Jia Wang³, and Matthew Davis¹

¹ ARC Centre of Excellence in Future Low-Energy Electronics and Technologies, University of Queensland, Queensland 4072, Australia

² ARC Centre of Excellence in Future Low-Energy Electronics and Technologies, Monash University, Victoria 3800, Australia

³ Centre for Quantum Technology and Theory, Swinburne University of Technology, Victoria 3122, Australia

* e.laird@uq.edu.au

Abstract

Pairing lies at the heart of superfluidity in fermionic systems. Motivated by recent experiments in mesoscopic Fermi gases, we study up to six fermionic atoms with equal masses and equal populations in two different spin states, confined in a quasi-two-dimensional harmonic trap. We couple a stochastic variational approach with the use of an explicitly correlated Gaussian basis set, which enables us to obtain highly accurate energies and structural properties. Utilising two-dimensional two-body scattering theory with a finite-range Gaussian interaction potential, we tune the effective range to model realistic quasi-two-dimensional scattering. We calculate the excitation spectrum, pair correlation function, and paired fraction as a function of increasing attractive interaction strength. For up to six fermions in the ground state, we find that opposite spin and momentum pairing is maximised well below the Fermi surface in momentum space. By contrast, corresponding experiments on twelve fermions have found that pairing is maximal at the Fermi surface and strongly suppressed beneath [M. Holten et al., *Nature* **606**, 287–291 (2022)]. This suggests that the Fermi sea — which acts to suppress pairing at low momenta through Pauli blocking — emerges in the transition from six to twelve particles.

Copyright attribution to authors.

This work is a submission to SciPost Physics.

License information to appear upon publication.

Publication information to appear upon publication.

Received Date

Accepted Date

Published Date

1

2 Contents

3	1 Introduction	2
4	2 Model	4
5	3 Results	7
6	3.1 Excitation Spectrum	7
7	3.2 Pair Correlation Function	9
8	3.3 Paired Fraction	15

9	3.4 Discussion	16
10	4 Conclusions and Outlook	17
11	A Method of Explicitly Correlated Gaussians	18
12	B Comparison to a Contact Interaction	22
13	C Definitions of the Pair Correlator and Density Matrices	23
14	D Derivation of the One-Body Terms in the Pair Correlator	24
15	E Derivation of the Two-Body Term in the Pair Correlator	28
16	F Bardeen–Cooper–Schrieffer (BCS) Theory	32
17	References	32
18		

19 1 Introduction

20 Fermionic superfluidity is a many-body phenomenon occurring in systems as diverse as liquid
 21 helium-three, superconductors, nuclear matter, neutron stars, and ultracold quantum gases.
 22 The key commonalities in these systems — that they flow without dissipation, have a non-
 23 classical rotational moment of inertia, and feature an energy gap in their elementary excitation
 24 spectrum — arise due to the pairing of fermions. Quantum gases provide an ideal experimental
 25 arena in which to interrogate the nature of fermion pairing since many of their degrees of
 26 freedom are highly tunable. Factors such as the number of particles, their internal states and
 27 interactions, the system dimensionality, and the confinement geometry can all be precisely
 28 measured and controlled [1–3]. In ultracold atomic Fermi gases, this has led to the realisation
 29 and detailed study of the crossover from a Bose–Einstein condensate (BEC) of tightly bound
 30 bosonic pairs to a Bardeen–Cooper–Schrieffer (BCS) superfluid of long-range Cooper pairs in
 31 three dimensions [4–11]. Restricting these gases to two dimensions strongly alters pairing and
 32 superfluidity [12–20], and may offer insight into unconventional forms of superconductivity
 33 encountered in solid-state physics [21, 22].

34 Very recently, S. Jochim’s group at Heidelberg University have experimentally probed how
 35 the key features of Fermi superfluidity emerge at the most fundamental level — ‘from the
 36 bottom up’ [23, 24]. The group deterministically prepared nearly pure quantum ground states
 37 for up to twenty ultracold fermions that were equally distributed between two different spin
 38 states and confined in a (quasi-)two-dimensional harmonic trap. Their flexible experimental
 39 set-up enabled them to tune the inter-spin interactions from the non-interacting limit into
 40 the regime of strong binding, and to extract the single particle and spin resolved momentum
 41 distribution of the Fermi gas at any intermediate interaction strength. They reported Cooper
 42 pairing in a system comprising only twelve interacting particles, which manifested as a peak
 43 in the correlations between atoms with opposing spins and momenta at the Fermi surface in
 44 momentum space [24]. In another experiment involving as few as six particles, they observed a
 45 few-body precursor of a quantum phase transition from a normal fluid to a superfluid [23]. The
 46 precursor transition was signalled by a softening (i.e., a decrease in frequency) of the lowest
 47 mode in the excitation spectrum when the attractive interaction strength was increased. In the
 48 many-body limit, this mode becomes associated with amplitude variations of the superfluid
 49 order parameter and is commonly referred to as the massive ‘Higgs mode’ [25]. While mode

50 softening in the six-atom system had previously been predicted [26], to our knowledge, the
51 pair momentum correlations mentioned above have not yet been theoretically calculated.

52 Earlier theoretical work on two-dimensional trapped mesoscopic Fermi gases has been
53 focused on probing their excitations. In 2016, G. Bruun et al. [26] calculated the monopole
54 (zero angular momentum) excitation spectra for between six and twelve fermions interacting
55 via a contact potential. For closed-shell configurations, they found that the lowest energy
56 mode depends non-monotonically on the interaction strength and mainly consists of coherent
57 excitations of time-reversed pairs — which, as mentioned above, has since been confirmed by
58 experiment [23]. Their approach employed the harmonic oscillator basis, which is convenient
59 for evaluating the Hamiltonian matrix elements, however is poor at approximating the cusps
60 in the wave function induced by the short-range interactions [27]. This made it necessary to
61 use very large numbers of basis states (on the order of $\sim 10^7$) to numerically converge the
62 energies [26], and the size of the calculation made it difficult to solve for two-body observables
63 such as momentum-space pair correlations. More recently in 2022, J. Hofmann et al. [28]
64 approximated the excitation spectra of the same Fermi systems by using an exactly solvable
65 (integrable) s -wave pairing Hamiltonian known as the Richardson model [29,30]. While a full
66 contact interaction can couple opposite spins in any combination of harmonic oscillator states,
67 the Richardson model only accounts for time-reversed pairing in the same energy level (or
68 shell) and assumes a constant coupling strength for all pairs. As such, the formalism retains the
69 key matrix elements that give rise to superfluidity [31] and allowed the lowest pair excitation
70 mode to be approximated for the first fifteen closed-shell configurations [28]. It was hence
71 demonstrated how the minimum energy of pair excitations deepens with increasing particle
72 number and shifts toward weaker interaction strengths, consistent with experiment [23].

73 In this manuscript, we adopt an entirely different and highly accurate (virtually exact)
74 approach for calculating the energetics of two-dimensional trapped mesoscopic Fermi gases,
75 which additionally allows us to determine their structural properties and pair correlation func-
76 tions. We obtain the excitation spectra variationally, based on the now renowned technique
77 introduced by K. Varga and Y. Suzuki in 1995 [32,33]. The trial wave functions are chosen
78 to be combinations of explicitly correlated Gaussians, which permit an analytical evaluation
79 of the Hamiltonian matrix elements [34,35]. The non-linear variational parameters of these
80 trial functions, the Gaussian widths, are selected stochastically. The suitability of this method
81 to describe ultracold few-particle systems is three-fold [36–38]: 1) Cold atoms are sufficiently
82 dilute that only binary interactions are important. Since each Gaussian basis function depends
83 explicitly on every two-body correlation (interparticle separation) in the system, a very high
84 accuracy is achievable. 2) Cold atoms have universal properties that are independent of the
85 microscopic details of the true interaction potential, justifying the assumption of a Gaussian
86 interaction. 3) The Gaussian basis functions are flexible enough to simultaneously replicate
87 correlations that develop on *any* length scale, including those of the scattering potential and
88 the external confinement. This is because a wave function in a harmonic trap has a natu-
89 rally Gaussian dependence at large distances, whereas its short-range cusp is well captured
90 by superpositions of Gaussians. Consequently, such an approach has previously been used to
91 obtain numerically exact energies and structural properties (such as radial one-body densities
92 and pair distribution functions, but not pair momentum correlations) for spin-balanced two-
93 component Fermi gases subject to an isotropic three-dimensional harmonic confinement. In
94 2011, the three-dimensional system was solved for up to six particles at a full range of interac-
95 tion strengths [39], while subsequently in 2014 and 2015, the eight- [40] and ten-particle [41]
96 problems were also solved at unitarity. For all three atom numbers, pairing could be evidenced
97 by the clear two-peak structure of the (scaled) radial pair distribution functions.

98 In the two-dimensional calculations reported here, we employ a shape-resonant Gaussian
99 interaction potential — which has a large and variable effective range — to mimic and probe

100 the *quasi*-two-dimensional nature of real experimental confinement geometries [42–45]. We
 101 are able to access the second-order pair correlations measured in experiment [24] by evalu-
 102 ating the matrix elements of the real-space one- and two-body fermionic density matrices in
 103 the correlated Gaussian basis and then analytically Fourier transforming the results into mo-
 104 mentum space. We focus on studying the correlations in the ground state for spin-balanced
 105 two-component Fermi gases in different interaction regimes. The one distinction between our
 106 theoretical analysis and the experiment is the number of particles. Whereas the latter involved
 107 twelve atoms, the maximum number that we can consider is six due to computational time
 108 constraints which are imposed by the first-quantised formulation of the explicitly correlated
 109 Gaussian (ECG) method. Nevertheless, our calculation of the pair correlation function is new
 110 and our findings complement the experiment in revealing how pairing emerges in the limit of
 111 very few fermions.

112 This paper is organised as follows: In Sec. 2 we discuss our model of the two-dimensional
 113 Fermi gas, including the special role played by the effective range of interactions. (Since the
 114 ECG method has already been thoroughly detailed in the literature, we distill the essential
 115 aspects which apply to solving the system of interest in Appendix A.) In Sec. 3 we present and
 116 interpret our results: First, we study the excitation spectrum of the Fermi gas, focusing on
 117 the unique behaviour of the lowest monopole mode. Subsequently, we elucidate the nature of
 118 opposite-spin pair correlations in the ground state and we directly compare our calculations
 119 to experiment. We investigate the effects of particle number, interaction strength, and axial
 120 confinement strength on both the excitations and pairing. We conclude and identify avenues
 121 for future research in Sec. 4.

122 2 Model

123 We theoretically consider equal-mass two-component Fermi gases comprising $N = N_\uparrow + N_\downarrow$
 124 atoms with balanced spin populations [i.e., $N_\uparrow = N_\downarrow = N/2$, where N_\uparrow (N_\downarrow) is the number of
 125 ‘spin-up’ (‘spin-down’) fermions]. Such a system is exemplified by ultracold fermionic atoms of
 126 ${}^6\text{Li}$ prepared in the two lowest ${}^2S_{1/2}$ hyperfine levels. In the experiments of interest, these par-
 127 ticles are confined to a highly anisotropic single layer of a standing-wave optical dipole trap,
 128 which freezes out motion along the axial (z) direction. This layer is then superimposed with
 129 an optical tweezer — or ‘microtrap’ — which provides an isotropic radial harmonic confine-
 130 ment ω_r , [23, 24, 46]. When superimposed on a large ensemble of atoms, the small microtrap
 131 can locally enhance the chemical potential by a significant amount without modifying the
 132 temperature of the gas [47]. This leads to a small region of increased densities deep in the
 133 degenerate regime, and due to Fermi–Dirac statistics, all low-lying energy levels of the micro-
 134 trap become filled with almost unit probability [46]. By inclining and lowering the trap walls
 135 in a controlled manner, particles above a certain ‘spill threshold’ can then be deterministically
 136 removed, leaving behind a stable *mesoscopic* number of atoms in the ground state [46]. The
 137 systems of particular relevance to the current study contain as few as $N_\uparrow + N_\downarrow = 1 + 1$, $2 + 2$,
 138 or $3 + 3$ particles, such that in the non-interacting ground state only the first two 2D harmonic
 139 oscillator shells are occupied. Interactions (collisions) subsequently induced by a Feshbach
 140 resonance between distinguishable fermions in the gas (i.e., between the different hyperfine
 141 states) are low in energy and well described by s -wave two-body physics.

142 The system Hamiltonian in two dimensions reads as follows:

$$\mathcal{H} = \sum_{i=1}^N \left[-\frac{\hbar^2}{2m} \nabla_{\mathbf{r}_i}^2 + V_{\text{ext}}(|\mathbf{r}_i|) \right] + \sum_{i < j}^N V_{\text{int}}(|\mathbf{r}_i - \mathbf{r}_j|), \quad (1)$$

143 where m is the atomic mass and \mathbf{r}_i denotes the position vector of the i^{th} atom measured from
 144 the trap centre. The first term corresponds to the kinetic energy of the particles, the second
 145 term to an external harmonic trap,

$$V_{\text{ext}}(|\mathbf{r}_i|) = \frac{m\omega_r^2}{2} r_i^2, \quad r_i \equiv |\mathbf{r}_i|, \quad (2)$$

146 and the third term to short-range pairwise interactions between fermions with unlike spins.
 147 We model these interactions with a finite-range Gaussian potential [45] that is parameterised
 148 by a width r_0 (> 0) and a depth V_0 (< 0):

$$V_{\text{int}}(|\mathbf{r}|) = V_0 \exp\left(-\frac{r^2}{2r_0^2}\right) - V_0 \frac{r}{l_r} \exp\left[-\frac{r^2}{2(2r_0)^2}\right], \quad (3)$$

149 where $l_r = \sqrt{\hbar/(m\omega_r)}$ is the radial harmonic oscillator length scale in the 2D plane. In the
 150 non-interacting limit of $V_0 = 0$, the Hamiltonian \mathcal{H} in Eq. (1) has eigenvalues of $\varepsilon^{(0)} = (2n +$
 151 $|m| + 1)\hbar\omega_r$, where $n = 0, 1, 2, \dots$ is the principal quantum number and $m = 0, \pm 1, \pm 2, \dots$
 152 is the quantum number for orbital angular momentum.

153 For a fixed value of r_0 , the value of V_0 can be adjusted to generate potentials with different
 154 free-space s -wave scattering lengths and effective ranges (or equivalently, we may fix V_0 and
 155 vary r_0). We consider two particles elastically scattering via the interaction potential, Eq. (3),
 156 in two-dimensional free space. We solve the s -wave radial Schrödinger equation for the relative
 157 motion up to a radius much larger than r_0 , matching the logarithmic derivatives of the wave
 158 functions to the asymptotic form in order to obtain the real-valued s -wave scattering phase
 159 shift $\delta(k)$ [48]. Subsequently, by fitting the phase shift to its low-energy expansion in two
 160 dimensions,

$$\cot[\delta(k)] = \frac{2}{\pi} \left[\gamma + \ln\left(\frac{ka_{2D}}{2}\right) \right] + \frac{1}{\pi} k^2 r_{2D} + \dots, \quad (4)$$

161 we determine both the s -wave scattering length a_{2D} and the effective range r_{2D} ¹ [49–51]. Here,
 162 $k \equiv |\mathbf{k}|$ is the magnitude of the relative wave vector between the two atoms in the 2D plane and
 163 $\gamma \simeq 0.577216$ is Euler's constant. At low energy, the physics is independent of the short-range
 164 details of the interaction potential and instead exhibits universality with respect to both a_{2D}
 165 and r_{2D} . Accordingly, in our calculations we choose Gaussian widths small enough, $r_0 \lesssim 0.1l_r$,
 166 to ensure that higher order expansion terms in Eq. (4) are negligible within the energy range
 167 of interest. We have furthermore implemented a modified version of the model potential —
 168 given by Eq. (S23) in the supplemental material of Ref. [45] — and have found that it yields
 169 the same energies as in Fig. 2 for a given two-body binding energy (defined below) and r_{2D} .
 170 This confirms that effects beyond those of the effective range are indeed negligible.

171 In two dimensions the scattering length is always positive, $a_{2D} > 0$. In a many-body pic-
 172 ture, the two-component Fermi gas undergoes a crossover from a Bose–Einstein condensate
 173 of diatomic molecules to a Bardeen–Cooper–Schrieffer superfluid of Cooper pairs as a_{2D} in-
 174 creases. However, unlike in three dimensions, there is no unitary limit where the system
 175 becomes scale invariant and the interaction strength (scattering length) diverges. Rather, the
 176 strongly interacting regime is in the vicinity of $\ln(k_F a_{2D}) = 0$, where the Fermi wave vector k_F
 177 denotes the radius of the non-interacting Fermi sea at zero temperature [52].

178 As previously described, in cold-atom experiments a two-dimensional geometry can be
 179 realised by applying a strong harmonic confinement along the axial direction, with angular

¹Note that the precise definitions of the two-dimensional scattering length a_{2D} and the two-dimensional effective range r_{2D} vary in the literature. Our particular definition of r_{2D} has units of squared length, consistent with Ref. [45].

180 frequency ω_z and length scale $l_z = \sqrt{\hbar/(m\omega_z)}$. Realistically, however, the extent of the gas
 181 perpendicular to the 2D plane is necessarily finite. At low energy and small l_z (such that
 182 $kl_z \ll 1$), the two-body scattering of distinguishable fermions can be mapped onto a 2D scat-
 183 tering amplitude with an effective range given by² [42–45]

$$r_{2D} = -l_z^2 \ln(2). \quad (5)$$

184 By assigning an appropriately finite and negative value to the effective range parameter in
 185 the purely two-dimensional model considered here, we can thus mimic the effect on the scat-
 186 tering of a *quasi*-two-dimensional confining potential. In particular, through our choice of the
 187 interaction parameters V_0 and r_0 , we can attribute a value to the dimensionless effective range
 188 r_{2D}/l_r^2 which matches the trap aspect ratio ω_z/ω_r in a given experiment.

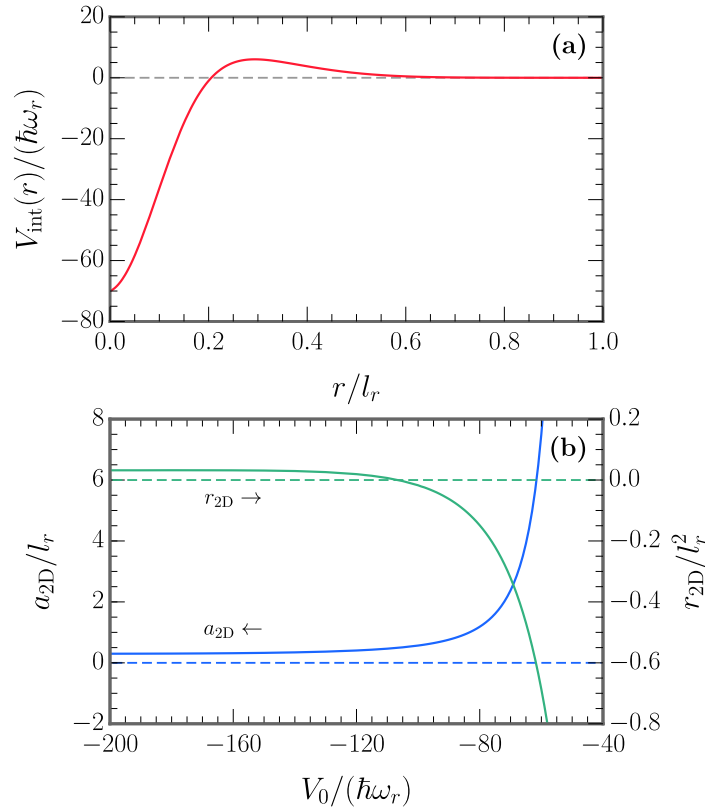


Figure 1: (a) The model Gaussian interaction potential, Eq. (3), at $V_0/(\hbar\omega_r) = -70$ and $r_0/l_r = 0.1$ [where $l_r^2 = \hbar/(m\omega_r)$]. (b) The two-dimensional scattering length a_{2D} (in blue) and the two-dimensional effective range r_{2D} (in green) as functions of the potential depth V_0 , for a fixed width of $r_0 = 0.1l_r$. (Note, this figure is similar to Fig. 1 in Ref. [45].)

189 In practical computations, we tune the effective range to large negative values through
 190 a shape resonance [45, 53], which arises due to the general structure of the model potential
 191 shown in Eq. (3): the first term creates an attractive well that can support virtual bound states,
 192 while the second term adds a small repulsive barrier that can couple these virtual bound states

²For this mapping to be valid, l_z is also required to be much greater than the van der Waals range of the interactions between atoms — i.e., $r_{\text{vdW}} \ll l_z < l_r$ — which is always satisfied experimentally.

193 to free-space scattering states — as depicted in Fig. 1(a). Figure 1(b) illustrates the range of
 194 combinations of a_{2D} and r_{2D} that can be obtained by fixing r_0 and varying V_0 . In this figure
 195 and in all our calculations, we restrict our attention to the regime where the potential supports
 196 a single two-body s -wave bound state in two-dimensional free space³ [45].

197 To numerically solve the time-independent Schrödinger equation for the Hamiltonian in
 198 Eq. (1), we employ the method of explicitly correlated Gaussians. A description of this tech-
 199 nique is provided in Appendix A. We parameterise our results in terms of the effective range r_{2D}
 200 and the two-body binding energy $\varepsilon_b > 0$, with the latter determined by the following approach.
 201 For every set of V_0 and r_0 values that we use to numerically solve a general $N_\uparrow + N_\downarrow$ problem,
 202 we also solve the corresponding $1 + 1$ problem numerically by implementing the correlated
 203 Gaussian method. This yields the relative energy of the two-body ground state, $\mathcal{E}_{\text{rel},1+1}$ (see
 204 Appendix A). The total ground-state energy of one spin- \uparrow particle and one spin- \downarrow particle in the
 205 2D harmonic trap is given by $\mathcal{E}_{1+1} = 2\hbar\omega_r - \varepsilon_b$. Since we know that $\mathcal{E}_{1+1} = \mathcal{E}_{\text{com},1+1} + \mathcal{E}_{\text{rel},1+1}$
 206 and there are no centre-of-mass excitations in the ground state, $\mathcal{E}_{\text{com},1+1} = \hbar\omega_r$, we can then
 207 immediately obtain ε_b .

208 3 Results

209 We apply the method of explicitly correlated Gaussians to obtain numerically optimised and
 210 converged basis sets at a wide range of attractive interaction strengths (or binding energies)
 211 for the fermionic systems of interest. Upon diagonalising the Hamiltonian, we utilise the eigen-
 212 values to calculate the low-energy excitation spectra of the Fermi gases and the eigenvectors
 213 to determine their structural properties. With regard to the latter, we focus on investigating
 214 the nature of opposite-spin pair correlations in the ground state and we directly compare our
 215 numerics against recent experimental measurements.

216 3.1 Excitation Spectrum

217 The excitation spectra of the Fermi systems are of fundamental interest since they can reveal
 218 signatures of pairing [26] and can be experimentally accessed in two dimensions [23]. Figure 2
 219 shows the lowest energy fermionic excitation spectrum, i.e., the difference ΔE between the
 220 first-excited-state and ground-state energies as a function of the two-body binding energy ε_b .
 221 In the upper panel (a) we compare our results for $N_\uparrow + N_\downarrow = 1 + 1, 2 + 2,$ and $3 + 3$ fermions at
 222 very nearly *zero* effective range (numerically, we set $r_{2D}/l_r^2 = -0.001 \approx 0$), while in the lower
 223 panel (b) our results for $3 + 3$ fermions are compared at *different* fixed values of the effective
 224 range.

225 The non-interacting ground state at $\varepsilon_b = 0$ can assume one of two configurations depend-
 226 ing on the total number of particles N : either all of the degenerate single-particle states of
 227 the highest energy level of the 2D harmonic oscillator are filled (‘closed shell’), or some of the
 228 degenerate states remain empty (‘open shell’). The $1 + 1$ and $3 + 3$ systems both feature a
 229 closed-shell ground state that is non-degenerate, whereas the $2 + 2$ ground state is open-shell.
 230 We restrict our consideration to ground states that are characterised by zero total orbital an-
 231 gular momentum. For the $2 + 2$ system, this means that the two highest energy opposite-spin
 232 fermions reside in different degenerate single-particle states. Since the Hamiltonian is rota-
 233 tionally symmetric, only monopole excitations between states with the same (i.e., zero) total

³At the point where a new bound state enters the potential both a_{2D} and $|r_{2D}|$ positively diverge. As discussed in Ref. [45], the potential does not support a two-body bound state in the limit of $V_0 \rightarrow 0$. In two dimensions this is in stark contrast to the case of a potential that is everywhere attractive. Such a potential (even one that is arbitrarily weak) always supports a two-body s -wave bound state in free space because the scattering amplitude always features a pole at negative energies [52].

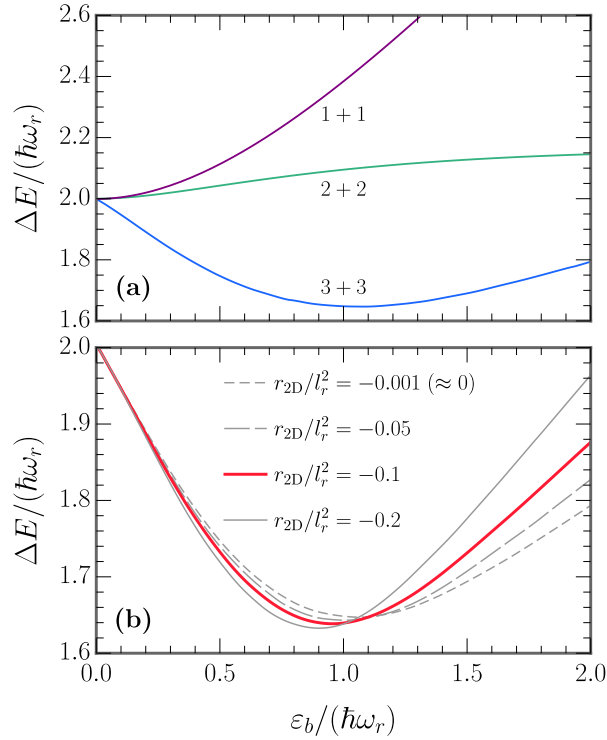


Figure 2: The lowest monopole excitation spectrum for various few-body Fermi systems. (a) The excitation energy ΔE as a function of the binding energy ε_b for $N_\uparrow + N_\downarrow = 1 + 1$, $2 + 2$, and $3 + 3$ fermions at zero effective range (i.e., $r_{2D}/l_r^2 = -0.001 \approx 0$). (b) The non-monotonic result for $3 + 3$ fermions at different effective ranges. The selected values $-r_{2D}/l_r^2 = -0.2, -0.1, -0.05, -0.001$ — respectively correspond to trap aspect ratios of $\omega_r/\omega_z \approx 1/3.5, 1/7, 1/14, 1/700$. [Note, the blue line in (a) is the same as the short-dashed gray line in (b).]

234 angular momentum occur⁴. For all three atom numbers at $\varepsilon_b = 0$, the lowest monopole exci-
 235 tation has an energy of $\Delta E = 2\hbar\omega_r$. This can be attributed either to exciting a single particle
 236 up two harmonic oscillator shells, or to exciting a time-reversed pair of particles (n, m, \uparrow) and
 237 $(n, -m, \downarrow)$ up one shell each.

238 As the attractive interaction strength increases from zero, $\varepsilon_b > 0$, the excitation energies
 239 for systems with different particle numbers in panel (a) evolve very differently. A striking fea-
 240 ture is the non-monotonic behaviour of ΔE for the case of $3 + 3$ fermions. As first argued in
 241 Ref. [26]⁵ — and later lucidly discussed in M. Holten’s PhD thesis [46] — this non-monotonicity
 242 is indicative of *pair correlations*. The first excited state for $3 + 3$ fermions is a linear combination
 243 of three degenerate configurations: one being the result of a single-particle excitation and the
 244 other two the result of pair excitations. The energy of the former grows with ε_b simply because
 245 increasing the mean-field attraction felt by each particle enhances the effective confinement,
 246 $\omega_r^{\text{eff}} > \omega_r$ — which thereby raises the cost of exciting a single particle, $\Delta E = 2\hbar\omega_r^{\text{eff}}$ [26]. On
 247 the other hand, when a pair of particles is excited from the closed-shell ground state they can
 248 use the degenerate states in the new, otherwise empty harmonic oscillator level to increase
 249 their wave function overlap. This causes them to gain binding energy, and hence, diminishes

⁴The m quantum numbers for all atoms sum to zero in both the ground and excited states.

⁵This work calculated the monopole excitation spectrum of the same system (but for contact interactions) by using exact diagonalisation in the harmonic oscillator basis.

250 the cost of monopole excitations monotonically as ε_b increases [26, 46]⁶. At a critical bind-
 251 ing energy the excitation energy ΔE reaches a minimum. Beyond this point the interaction
 252 strength becomes comparable to the radial trapping frequency $\varepsilon_b \sim \hbar\omega_r$, which signifies that
 253 pairing then occurs not only in the excited states, but also in the ground state. As a result,
 254 the ground-state energy starts decreasing faster than the first-excited-state energy, such that
 255 ΔE begins to increase [23]. These pairing effects are dominant in the 3 + 3 system which
 256 leads to the overall non-monotonic dependence of ΔE on ε_b . This is not the case for 1 + 1
 257 and 2 + 2 fermions in the monopole sector, and consequently, for those systems ΔE increases
 258 monotonically with ε_b instead. In Appendix B, we discuss how our results based on the Gaus-
 259 sian interaction potential of Eq. (3) compare quantitatively to the contact interaction results
 260 from Ref. [26].

261 For systems with a closed-shell ground state, the minimum value of ΔE at the critical
 262 binding energy decreases as the number of particles increases, until in the many-body limit
 263 ($N \rightarrow \infty$) it reduces to zero and pairs are coherently excited without any energy cost [25, 26].
 264 When ε_b is increased from zero to this critical value, the many-body two-component Fermi
 265 gas becomes unstable and undergoes a second-order phase transition into a superfluid state.
 266 The lowest energy monopole excitation of the trapped superfluid corresponds to the Higgs
 267 mode which has an energy equal to twice the superfluid gap [25, 46]. Our result for 3 + 3
 268 fermions in panel (a) can thus be viewed as a *few-body precursor* to the Higgs mode for the
 269 Gaussian interaction potential given by Eq. (3). In panel (b), we investigate the effect of differ-
 270 ent quasi-two-dimensional harmonic confinements on this ‘few-body Higgs mode’ by varying
 271 the effective range parameter r_{2D} introduced in Eq. (4). We plot the lowest monopole excita-
 272 tion energy for 3 + 3 fermions at the following effective ranges: $r_{2D}/l_r^2 = -0.2, -0.1, -0.05,$
 273 -0.001 — which, according to Eq. (5), are associated with trap aspect ratios of: $\omega_r/\omega_z \approx$
 274 $1/3.5, 1/7, 1/14, 1/700$, respectively. Notably, we find that as the magnitude of the nega-
 275 tive effective range increases, the minimum of ΔE decreases and also shifts to smaller bind-
 276 ing energies ε_b . Moreover, the dependence of ΔE on r_{2D} (or l_z) becomes less significant
 277 at smaller ε_b . The experiment against which we will later compare our calculated pair mo-
 278 mentum correlations had radial and axial trapping frequencies of $\omega_r = 2\pi \times 1,101$ Hz and
 279 $\omega_z = 2\pi \times 7,432$ Hz [24]. These correspond to an aspect ratio of $\sim 1/7$ and an effective range
 280 of $r_{2D}/l_r^2 = -0.1027 \approx -0.1$ — designated by the thick red line in panel (b).

281 3.2 Pair Correlation Function

282 Pairing — regardless of the exact mechanism by which the particles attract each other — is
 283 a correlation phenomenon. This means that we can extract its description from the quantum
 284 two-body density matrix, which contains a complete set of information on all two-body corre-
 285 lations in the system [54]. In the position representation, the two-body density matrix reads
 286 as follows:

$$\rho(\mathbf{r}_1, \mathbf{r}'_1; \mathbf{r}_2, \mathbf{r}'_2) = \langle \psi_\uparrow^\dagger(\mathbf{r}_1) \psi_\uparrow(\mathbf{r}'_1) \psi_\downarrow^\dagger(\mathbf{r}_2) \psi_\downarrow(\mathbf{r}'_2) \rangle, \quad (6)$$

287 where $\langle \dots \rangle$ denotes an expectation value, and $\psi_\sigma^\dagger(\mathbf{r})$ and $\psi_\sigma(\mathbf{r})$ are fermionic field creation
 288 and annihilation operators, respectively (with $\sigma = \uparrow, \downarrow$). The diagonal matrix elements of
 289 Eq. (6) correspond to the instantaneous correlations between all particles’ positions, whereas
 290 the off-diagonal elements are responsible for two-particle coherence [54]. The diagonal ele-
 291 ments are of particular interest since they are directly accessible in experiments. These ele-

⁶Similarly, the remaining pairs of particles in the lower harmonic oscillator shell can increase their wave function overlap and gain binding energy by occupying the degenerate states that are now free. Thus, the pair excitation energy is a many-particle quantity that can only be accurately determined by taking the entire mesoscopic sample into account [46].

292 ments, $\langle \eta_\uparrow(\mathbf{r}_1)\eta_\downarrow(\mathbf{r}_2) \rangle$ — written using the density operator, $\eta_\sigma(\mathbf{r}) = \psi_\sigma^\dagger(\mathbf{r})\psi_\sigma(\mathbf{r})$ — speci-
 293 cally provide the probability of simultaneously finding opposite-spin fermions at positions \mathbf{r}_1
 294 and \mathbf{r}_2 . They can equivalently be written as $\langle n_\uparrow(\mathbf{p}_1)n_\downarrow(\mathbf{p}_2) \rangle$ — with $n_\sigma(\mathbf{p} = \hbar\mathbf{k})$ the momentum-
 295 space density operator — in order to give the probability of simultaneously finding opposite-
 296 spin fermions with momenta \mathbf{p}_1 and \mathbf{p}_2 . Since the signatures of opposite-spin pairing are
 297 predominantly evident in the momentum correlations, we focus on the latter. Note that even
 298 in the purely non-interacting regime, coincidences of a spin- \uparrow fermion with momentum \mathbf{p}_1 and
 299 a spin- \downarrow fermion with momentum \mathbf{p}_2 can still occur. In this limit, the two-particle density dis-
 300 tribution becomes a direct product of independent single-particle densities: $\langle n_\uparrow(\mathbf{p}_1)n_\downarrow(\mathbf{p}_2) \rangle =$
 301 $\langle n_\uparrow(\mathbf{p}_1) \rangle \langle n_\downarrow(\mathbf{p}_2) \rangle$ [54]. We therefore subtract this quantity so as to only account for correla-
 302 tions caused solely by interactions, leading to the second-order correlation function, $\mathcal{C}^{(2)}$, that
 303 features in S. Jochim’s experiments [24]:

$$\mathcal{C}^{(2)}(\mathbf{p}_1, \mathbf{p}_2) = \langle n_\uparrow(\mathbf{p}_1)n_\downarrow(\mathbf{p}_2) \rangle - \langle n_\uparrow(\mathbf{p}_1) \rangle \langle n_\downarrow(\mathbf{p}_2) \rangle. \quad (7)$$

304 We theoretically evaluate $\mathcal{C}^{(2)}$ by using the method of explicitly correlated Gaussians, relegat-
 305 ing the details of this calculation to the appendices, while focusing the main text on a discus-
 306 sion of our results. In Appendix C, we define the expectation values in Eq. (7) in terms of the
 307 one- and two-body fermionic density matrices in position and momentum space. The real-
 308 space one-body density matrix in the correlated Gaussian basis has previously been derived in
 309 Ref. [39] for the case of an isotropic three-dimensional harmonic confinement. In Appendix D,
 310 we perform the analogous derivation in two dimensions and then analytically Fourier trans-
 311 form the result to determine expressions for $\langle n_\uparrow(\mathbf{p}_1) \rangle$ and $\langle n_\downarrow(\mathbf{p}_2) \rangle$. In Appendix E, we extend
 312 this approach to obtain the correlated Gaussian matrix elements of the real-space two-body
 313 density matrix. The Fourier transformation into momentum space can again be carried out
 314 analytically to yield an expression for $\langle n_\uparrow(\mathbf{p}_1)n_\downarrow(\mathbf{p}_2) \rangle$.

315 A pertinent question is how to define (or approximate) the Fermi momentum $p_F = \hbar k_F$
 316 in a few-body system. The harmonic trap in the radial direction provides not only a natural
 317 length scale for the Fermi gas $l_r = \sqrt{\hbar/(m\omega_r)}$, which sets the average interparticle spacing,
 318 but also a natural momentum scale $p_r = \sqrt{\hbar m\omega_r}$. When there are only very few particles, the
 319 step in the momentum distribution at p_F for a given spin component is ‘smeared out’, with a
 320 width on the order of p_r . Thus, while the mesoscopic sample is characterised by two distinct
 321 momentum scales p_r and p_F , an unambiguous definition of p_F does not exist because the Fermi
 322 surface is coarse-grained [46]. One option in this case is to simply use the continuum equation
 323 which typically defines the Fermi momentum in a many-body system $p_F = \sqrt{2m\varepsilon_F}$, where the
 324 Fermi energy ε_F is the energy of the non-interacting ground state at zero temperature. Instead,
 325 we choose to define p_F in a manner consistent with Ref. [55] which also theoretically probes
 326 the many-body physics of two-component Fermi gases from the few-body regime. Therein the
 327 authors employ the local density approximation (LDA) in three dimensions to determine p_F
 328 as a smooth function of the number of particles $N \leq 10$. Although the applicability of either
 329 the continuum equation or the LDA to such small atom numbers may be questioned, the latter
 330 approach minimises few-body shell effects and smoothly extrapolates to the correct result in
 331 the large- N limit. We therefore define a local chemical potential $\mu(\mathbf{r}) = \mu - V_{\text{ext}}(|\mathbf{r}|)$, which
 332 depends on the global chemical potential $\mu = \partial\varepsilon/\partial N$, where ε is the total energy of the trapped
 333 gas. In two dimensions, a trapped non-interacting Fermi gas with balanced spin populations
 334 has the particle number density,

$$n(\mathbf{r}) = \frac{m}{\pi} \left(\mu - \frac{m\omega_r^2}{2} r^2 \right), \quad (8)$$

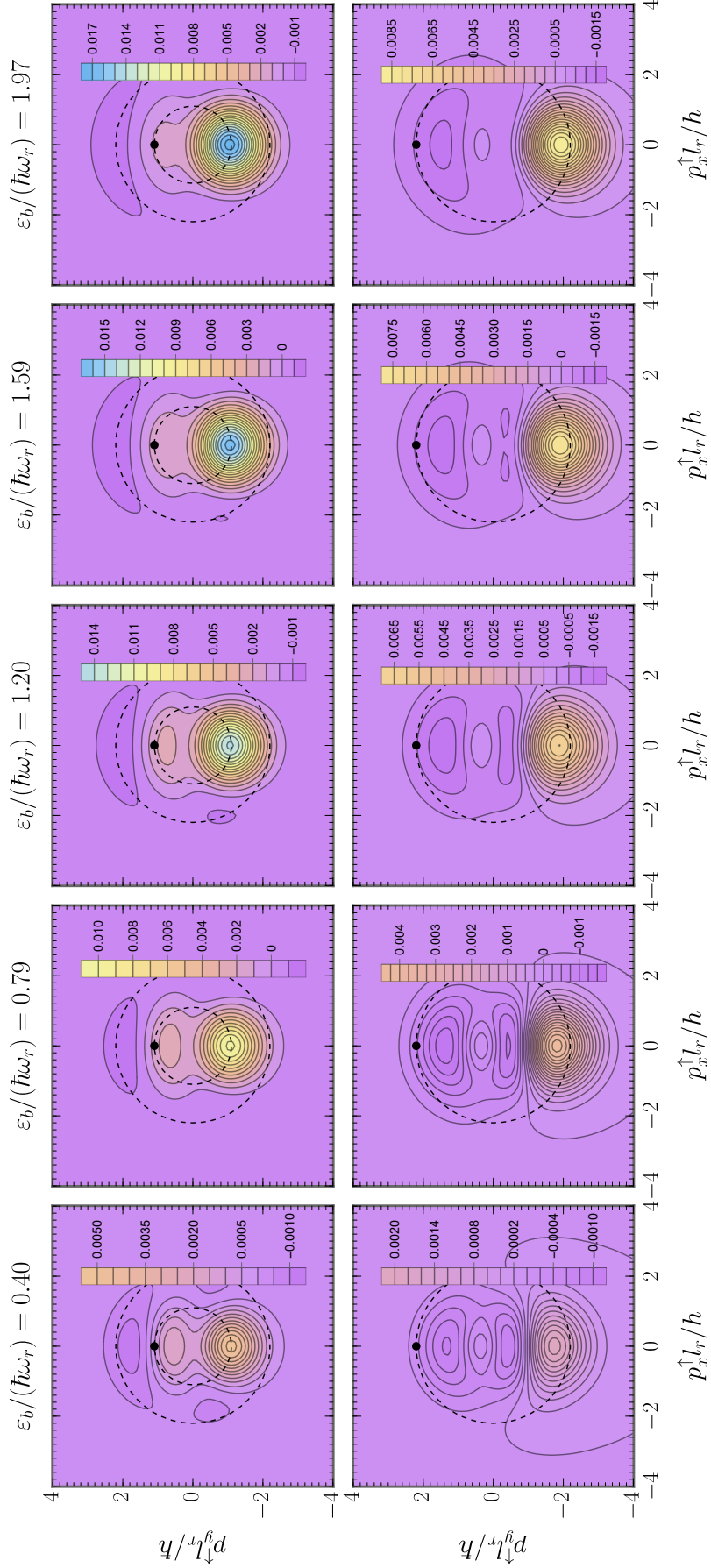


Figure 3: $C^{(2)}(\mathbf{p}_\uparrow, \mathbf{p}_\downarrow)$ as a function of \mathbf{p}_\uparrow with \mathbf{p}_\downarrow fixed at the black point for 3 + 3 fermions in the ground state. The radii of the dashed circles signify $|\mathbf{p}_\downarrow|$ and p_F .

335 which gives the total number of particles,

$$N = 2N_{\uparrow} = \int d^2\mathbf{r} n(\mathbf{r}) = \frac{\mu^2}{\omega^2}. \quad (9)$$

336 Above, the radial co-ordinate $r \equiv |\mathbf{r}|$ is integrated from zero up to the Thomas–Fermi radius
337 $r_{\text{TF}} = \sqrt{2\mu/(m\omega_r^2)}$. By using the definition of the trap length l_r , we then immediately obtain

$$p_F = (8N_{\uparrow})^{1/4} \hbar/l_r \quad (10)$$

338 as the local Fermi momentum at the centre of the trap.

339 We first take the correlation function $C^{(2)}(\mathbf{p}_1, \mathbf{p}_2)$ in Eq. (7) and fix \mathbf{p}_2 to a single value
340 denoted by $\bar{\mathbf{p}}_2$, while allowing \mathbf{p}_1 to vary. We plot the results for the ground state of the $N_{\uparrow} +$
341 $N_{\downarrow} = 3 + 3$ Fermi system in Fig. 3. The effective range is set to the experimental value in all
342 panels, $r_{2D}/l_r^2 = -0.1$, and the binding energy increases across the panels from left to right.
343 We consider all (non-zero) binding energies measured in Fig. 2 of Ref. [24]: $\varepsilon_b/(\hbar\omega_r) =$
344 $0.79, 1.20, 1.97$ — except for $\varepsilon_b/(\hbar\omega_r) = 15.90^7$ — and two additional intermediate values:
345 $\varepsilon_b/(\hbar\omega_r) = 0.40, 1.59$. The horizontal and vertical axes on each plot respectively measure
346 the x and y components of $\mathbf{p}_1 \equiv \mathbf{p}_{\uparrow}$. The value of $\bar{\mathbf{p}}_2 \equiv \bar{\mathbf{p}}_{\downarrow}$ is indicated by the black point
347 (\bullet) and a dashed circle is drawn at that radius, while another dashed circle is drawn at the
348 radius of the Fermi momentum p_F . In the upper panels $\bar{\mathbf{p}}_2$ is located inside the Fermi sea,
349 whereas in the lower panels it is positioned on the Fermi surface. All panels utilise the same
350 colour scaling. Our figure can be directly compared to plots (a)–(j) in Fig. 2 of Ref. [24]. As
351 was found in experiment, for particles with different spins there are only considerable second-
352 order correlations between those which have opposing momenta. However, in contrast to
353 the experiment we see that pairing in the $3 + 3$ system is dominant inside the Fermi sea, rather
354 than on the Fermi surface, at all considered binding energies. The experiment for $6 + 6$
355 fermions instead showed pairing to be dominant on the Fermi surface at binding energies of
356 $\varepsilon_b/(\hbar\omega_r) = 0.79, 1.20$, and 1.97 .

357 In view of Fig. 3, we define the opposite-momentum pair correlator as $C^{(2)}(\mathbf{p}_1 = \mathbf{p}, \mathbf{p}_2 =$
358 $-\mathbf{p})$, as was done in Ref. [24]. Due to radial symmetry, $C^{(2)}(\mathbf{p}, -\mathbf{p}) \equiv C^{(2)}(p)$ only depends
359 on the magnitude of the particles' momenta and can thus be expressed as a one-dimensional
360 correlation function. $C^{(2)}(p)$ is plotted in its dependence on momentum p for $3 + 3$ fermions
361 in the ground state in Fig. 4. We explore the parameter space by varying both the two-body
362 binding energy ε_b and the effective range r_{2D} . Each panel is associated with one of the bind-
363 ing energies previously considered in Fig. 3. Inside a given panel, the thick red line corre-
364 sponds to the experiment's value of the effective range, $r_{2D}/l_r^2 = -0.1$, whereas the thin gray
365 lines correspond to the other effective ranges featured in the excitation spectra of Fig. 2(b).
366 [Note that in every panel of Fig. 4, there is one point along the red curve that matches with
367 one point in the associated 2D contour plot of Fig. 3 (with the same binding energy) — but
368 otherwise, these figures contain different information.] Similar to in Ref. [24], we include as
369 a green line the limit from standard BCS theory (normalised to the correct number of parti-
370 cles), which is valid when the mean-field superfluid gap greatly exceeds the binding energy:
371 $\Delta = \sqrt{2\varepsilon_b\varepsilon_F} \gg \varepsilon_b$ [12], where $\varepsilon_F = p_F^2/(2m)$ denotes the Fermi energy. While this result
372 is not quantitatively accurate for only six (or twelve) particles because it neglects quantum

⁷At this binding energy, the $6+6$ system in the experiment formed bosonic pairs that were strongly interacting [24]. In the BEC limit of even higher binding energies, the particles would form non-interacting point-like molecules that reside in the ground state of the harmonic oscillator [11]. Later in Fig. 6 where we determine the paired fraction in the $3 + 3$ ground state, we will see that we are never close to the deep BEC regime for our considered range of binding energies, $\varepsilon_b \lesssim 2\hbar\omega_r$. At $\varepsilon_b > 2\hbar\omega_r$ — even using the flexible ECG approach — it is difficult to properly model the tight composite bosonic wave functions, and thus, to obtain *fully* numerically converged energies and structural properties within a reasonable time frame.

373 fluctuations, it nonetheless provides a qualitative picture of the many-body limit — namely, a
 374 single peak at the Fermi momentum p_F . The details of the BCS calculation can be found in
 375 Ref. [24] and are reproduced here in Appendix F for completeness.

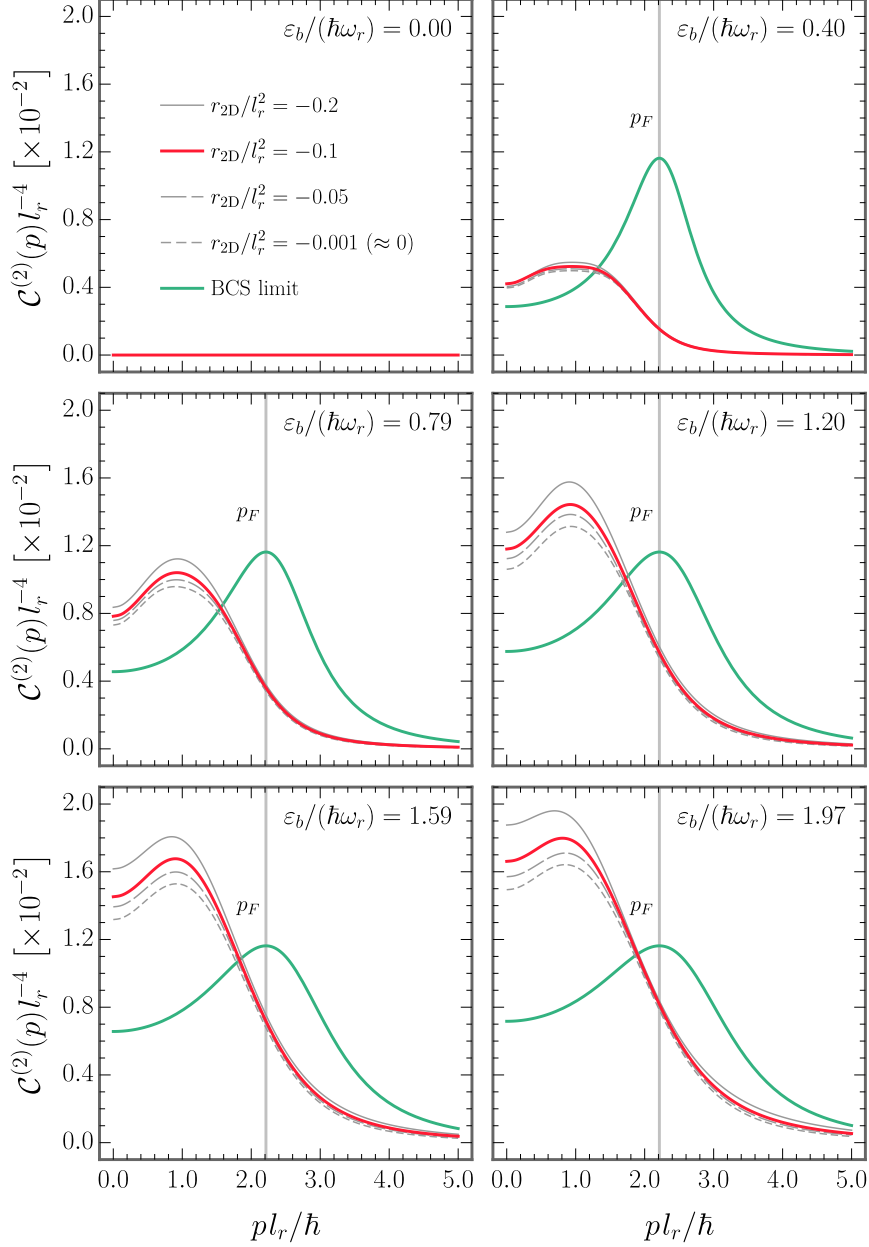


Figure 4: The calculated opposite-momentum pair correlator $\mathcal{C}^{(2)}(p)$ as a function of momentum p for the ground state of $N_{\uparrow} + N_{\downarrow} = 3 + 3$ fermions. The multiple panels are associated with different interaction strengths $\sim \varepsilon_b$, whereas the axial confinement $\sim r_{2D}$ is varied within each panel. In the experiment of Ref. [24] the measured binding energies were $\varepsilon_b/(\hbar\omega_r) = 0.00, 0.79, 1.20,$ and 1.97 , while the trap aspect ratio corresponded to an effective range of $r_{2D}/l_r^2 = -0.1$ (marked by the thick red line). The vertical gray line designates the Fermi momentum p_F .

376 Across all panels of Fig. 4, we observe that the strength of the correlations (the maximum
 377 height of the peak) increases with increasing binding energy. This aligns with expectations
 378 that larger binding energies (or interaction strengths) lead to an increase in pairing. On the
 379 other hand, the horizontal position of the peak's maximum barely changes with the binding
 380 energy. Within a panel, we see that increasing the magnitude of the negative effective range
 381 (at a fixed binding energy) also enhances the pair correlations. But again, this does not shift
 382 the peak horizontally. We therefore conclude that opposite spin and momentum pairing for
 383 3 + 3 fermions is consistently largest at momenta significantly below the Fermi surface. This
 384 again contrasts with the experimental measurements for 6 + 6 fermions [24], where $C^{(2)}(p)$
 385 was observed to peak at $p = p_F$ for the same range of binding energies, $\varepsilon_b \lesssim 2\hbar\omega_r$.

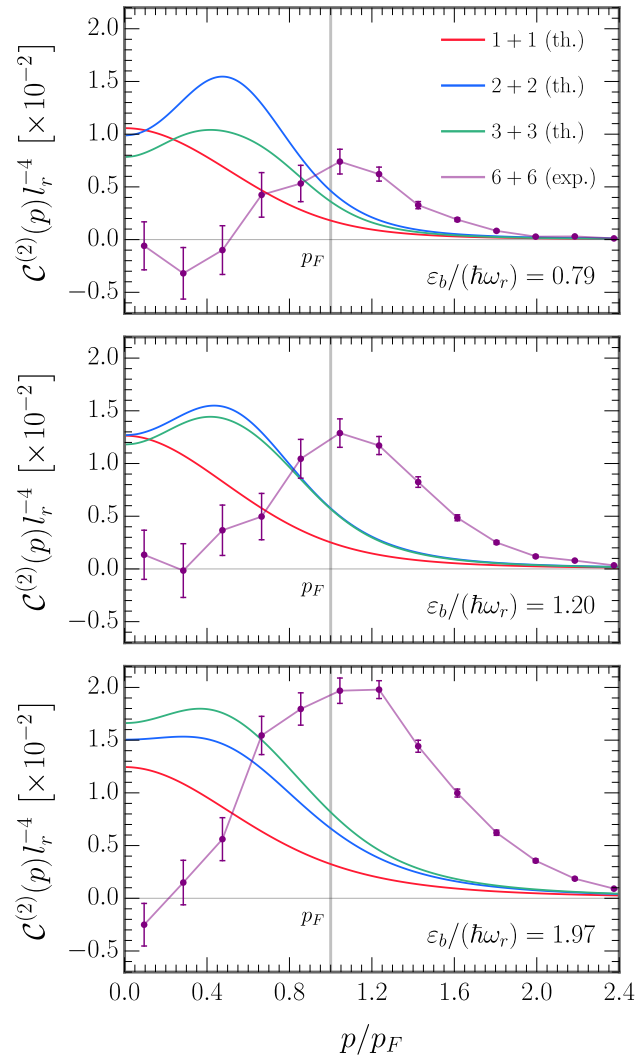


Figure 5: The opposite-momentum pair correlator $C^{(2)}(p)$, plotted as a function of the rescaled momentum p/p_F , and compared for different particle numbers. Each panel corresponds to a different binding energy ε_b . The smooth red, blue, and green curves are the theoretical results for $N_\uparrow + N_\downarrow = 1 + 1$, $2 + 2$, and $3 + 3$ fermions in the ground state, respectively (at the experiment's value of the effective range, $r_{2D}/l_r^2 = -0.1$), while the purple line is the experimental data for the 6 + 6 fermion ground state. The vertical grey line designates the Fermi momentum p_F .

386 In Fig. 5, we overlay the theoretical results on the experimental measurements mentioned
 387 above at binding energies of $\varepsilon_b/(\hbar\omega_r) = 0.79, 1.20,$ and 1.97 — taken from plots (l), (m),
 388 and (n) in Fig. 2 of Ref. [24]. In each panel the smooth red, blue, and green curves show the
 389 calculated opposite-momentum pair correlator $\mathcal{C}^{(2)}(p)$ as a function of momentum p for the
 390 ground state of $1+1, 2+2,$ and $3+3$ fermions, respectively (with $r_{2D}/l_r^2 = -0.1$). The purple
 391 line is the experimental data for the $6+6$ ground state. To properly compare systems with
 392 different particle numbers we rescale the momentum along the horizontal axis by the Fermi
 393 momentum p_F . [Note that our definition of the Fermi momentum, Eq. (10), differs slightly
 394 from the continuum definition used in Ref. [24]. For $6+6$ ($3+3$) fermions this difference is only
 395 about 7% (10%).] Due to the rescaling, we can see that qualitatively — and quantitatively at
 396 large momenta, $p > p_F$ — there is minimal difference in the pairing between the $2+2$ and $3+3$
 397 systems. This may be related to the fact that the non-interacting ground state for both four and
 398 six particles involves the same number of harmonic oscillator shells. Notably, the experimental
 399 $\mathcal{C}^{(2)}(p)$ function peaks at p_F and vanishes at $p \rightarrow 0$ ⁸, while the theoretical $\mathcal{C}^{(2)}(p)$ function for
 400 fewer particles peaks well below the Fermi surface and remains finite at small momenta. We
 401 remark that the depicted $\mathcal{C}^{(2)}(p)$ results for $1+1$ fermions have been compared to the results
 402 of another method of exact diagonalisation which uses a numerical B-spline basis set⁹, and in
 403 all cases, the agreement was found to be exact.

404 3.3 Paired Fraction

405 We can compute the number of opposite-momentum pairs, N_{pair} , by integrating $\mathcal{C}^{(2)}(p)$ over
 406 two-dimensional momentum space. In Fig. 6, we plot N_{pair} (red points) as a function of in-
 407 teraction strength ε_b for the $3+3$ closed-shell ground state (with $r_{2D}/l_r^2 = -0.1$). This figure
 408 directly illustrates how the system evolves from an unpaired to a paired state. The maximum
 409 possible number of pairs, $N_{\text{pair}} = 3$, is attainable in the deep BEC limit. Here, we see that for
 410 weak-to-moderate interactions only a small fraction of the system is paired. The analogous
 411 experimental data for the $6+6$ closed-shell ground state is provided in Fig. 3 of Ref. [24]. In
 412 a closed-shell structure, all the energy levels up to the Fermi energy are fully occupied and
 413 there is a gap of $\hbar\omega_r$ between the completely filled and completely empty levels. This energy
 414 gap stabilises the state against small perturbations, and consequently, pairing is suppressed at
 415 small binding energies, $\varepsilon_b \ll \hbar\omega_r$ [46]. A critical binding energy ε_b^c must be reached before
 416 it becomes energetically favourable to excite fermions into the empty higher levels and form
 417 pairs [46]. In the many-body limit ($N \rightarrow \infty$), the system remains in the normal state for
 418 $\varepsilon_b \ll \hbar\omega_r$ and undergoes a quantum phase transition to a superfluid state with long-range or-
 419 der at ε_b^c . On the mesoscopic scale a precursor of this phase transition can be observed in the
 420 fermionic excitation spectra, as we discussed in Sec. 3.1 [23, 26]. The critical binding energy
 421 for $3+3$ fermions is associated with the minimum energy of the lowest monopole excitation
 422 in Fig. 2(b) — for $r_{2D}/l_r^2 = -0.1$ (i.e., the red curve) this value is $\varepsilon_b^c \approx 0.953\hbar\omega_r$. The pre-
 423 diction for N_{pair} from standard mean-field BCS theory (see either Ref. [24] or Appendix F) is
 424 given by the solid blue line in Fig. 6. In order to describe mesoscopic samples, the authors of
 425 Ref. [24] off-set the BCS result by the critical binding energy as a type of first-order approxi-
 426 mation of finite-size effects. In Fig. 6, we find that the shifted model (dashed green line) fits
 427 our numerics (red points) very well for $\hbar\omega_r \lesssim \varepsilon_b \lesssim 2\hbar\omega_r$. Below this however, the grand

⁸It should be noted that the error bars on the experimental data in Fig. 5 are much larger at small momenta than at high momenta. This is because $\mathcal{C}^{(2)}(p)$ is experimentally determined by ‘counting’ pairs of atoms with opposite spins and momenta that occur anywhere around a ‘ring’ of radius p in momentum space, and then dividing by that radius. Due to a purely statistical effect, at very small radii the numbers of counts are also very small, which means those data points are inherently less reliable.

⁹B-splines are piece-wise polynomials which can be defined through recursive relations [56]; for a review of their application to quantum atomic and molecular physics, consult Ref. [57].

428 canonical ensemble on which the model is based leads to a sharp onset of pairing at ε_b^c [24].
 429 By contrast, we see that the 3+3 system smoothly transitions into a paired state for $\varepsilon_b > 0$ due
 430 to the small fixed particle number. A similar smooth transition was observed for the 6+6 sys-
 431 tem [24], corroborating how the ground-state paired fraction evolves with interaction strength
 432 in mesoscopic Fermi gases.

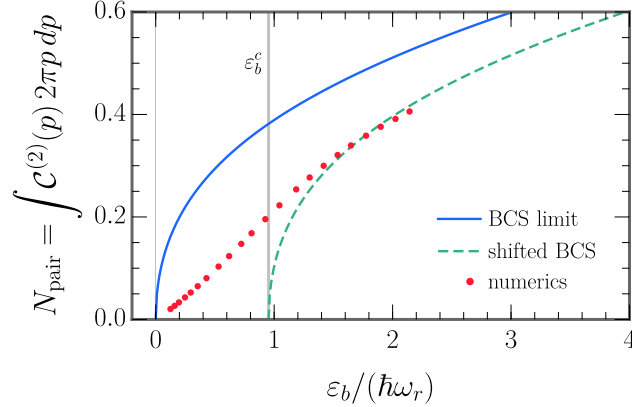


Figure 6: The number of opposite-momentum pairs N_{pair} (red points) as a function of interaction strength ε_b for the 3+3 fermion ground state (with $r_{2D}/l_r^2 = -0.1$). At larger binding energies, the mesoscopic sample can be accurately described by shifting the result from standard BCS theory by the critical binding energy, $\varepsilon_b^c \approx 0.953\hbar\omega_r$ (vertical gray line) [24].

433 3.4 Discussion

434 By comparing the results for the pair correlation function of Sec. 3.2 with those from the ex-
 435 periment in Ref. [24], one could surmise that the transition from an atomic Fermi system with
 436 few-body pairing to one with (qualitatively) many-body pairing occurs somewhere between
 437 six and twelve particles. We point out that in two dimensions, as was eloquently discussed in
 438 Ref. [58], there is a strong connection between the few- and many-body physics of fermion
 439 pairing: Elementary quantum mechanics shows that for two isolated particles in a vacuum
 440 (such as two distinguishable spin-1/2 fermions), a bound state always exists for an arbitrarily
 441 weak, purely attractive interaction [58]. It can also be shown that the existence of a two-body
 442 bound state for isolated particles is a necessary and sufficient condition for the Cooper insta-
 443 bility of the many-body Fermi sea [12]. This connection is not present in three dimensions:
 444 In that case, the interactions must reach a threshold strength before they are able to bind two
 445 isolated particles. This means that pairing at arbitrarily weak interactions in three dimensions
 446 must be entirely attributed to many-body effects [58]. When the two fermions are on top of
 447 a non-interacting filled Fermi sea, rather than in vacuum, the density of available scattering
 448 states is altered due to the presence of the other atoms. Momentum states beneath the Fermi
 449 surface are unavailable due to Pauli blocking, and at weak interactions, the particles' momenta
 450 are restricted to a narrow shell just above the Fermi surface. The three-dimensional density of
 451 states is proportional to the square root of the energy $\rho_{3D}(\varepsilon) \propto \sqrt{\varepsilon}$, but at the Fermi surface
 452 it becomes constant $\rho_{3D}(\varepsilon_F)$ just like in two dimensions. The effectively reduced dimension-
 453 ality of the system hence allows the formation of a two-body bound state for arbitrarily weak
 454 attraction [58, 59].

455 In the many-body regime, Cooper pairing tends to be concentrated at the Fermi surface
 456 regardless of whether the system is two- or three-dimensional. This is because any two distin-
 457 guishable particles need to scatter in order to pair (i.e., to become entangled). Likewise, the
 458 system needs to build up a superposition of many momenta in order to form a paired state.
 459 (This is made clear, for example, by recalling the structure of the ansatz for the superfluid
 460 ground-state wave function in standard BCS theory [59, 60].) However, Pauli blocking pre-
 461 vents these processes from happening deep inside the Fermi sea. For the Fermi sea to pair,
 462 some scattering states would need to be made available at low momenta — and this would
 463 require removing some particles from the Fermi sea by scattering them across a large momen-
 464 tum. The attractive interactions must therefore become strong enough to make it energetically
 465 favourable for those particles to scatter out. For weak-to-moderate interactions pairing is hence
 466 localised at the Fermi surface due to Pauli blocking, but begins to spread deeper into the Fermi
 467 sea as the interaction strength increases [59]. For very strong interactions the Fermi surface
 468 completely breaks up and pairing occurs at all momenta. In this limit the many-body system
 469 transitions from Cooper pairs to molecules [24, 60].

470 Having only very few particles thus leads to the question of how strong is the Pauli block-
 471 ing effect of the Fermi sea? Indeed, the extent of the occurrence of Pauli blocking can be con-
 472 sidered a measure of the extent to which the system can be legitimately called a ‘Fermi sea’.
 473 Because the experimental $C^{(2)}(p)$ function peaks at the Fermi momentum p_F for a wide range
 474 of interaction strengths, $\varepsilon_b \lesssim 2\hbar\omega_r$, this suggests that $6 + 6$ fermions is already approaching
 475 the number of particles required for a quantum many-body system and essentially constitutes
 476 a Fermi sea. By contrast, the theoretical $C^{(2)}(p)$ function peaks substantially below the Fermi
 477 momentum in the same interaction regime. This indicates that $3 + 3$ fermions is still a few-body
 478 system in which the low-momentum states are paired. It would therefore be of considerable
 479 interest to extend our calculations to $4 + 4$, $5 + 5$, and $6 + 6$ particles to confirm this interpre-
 480 tation. Alternatively, it would be interesting to experimentally measure the pair correlation
 481 function for a number of particles smaller than $6 + 6$ [24] to compare against our results. As
 482 we discuss in Appendix A, the main burden on computational time for increasing particle num-
 483 ber is the rapid increase in the number of permutations required to antisymmetrise the wave
 484 function — which currently limits our investigation to $3 + 3$ atoms. If the $6 + 6$ calculation
 485 were feasible timewise, then the additional full harmonic oscillator shell in the non-interact-
 486 ing ground state may be enough to qualitatively modify the outcome from the $3 + 3$ case. In
 487 three dimensions, energies and some structural properties (but not opposite-momentum pair
 488 densities) have previously been obtained for $4 + 4$ [40] and $5 + 5$ [41] fermions at unitarity
 489 by using basis sets that account for the most important but not all correlations. However, this
 490 approach may be less accurate at weak-to-moderate interactions. Besides particle number, an-
 491 other factor which may have played a role in the difference of results is temperature, i.e.,
 492 our calculations assumed zero temperature, while the experiment was performed at a finite
 493 temperature which led to a ground-state fidelity of 76% [24]. Nevertheless, we expect this to
 494 be less significant since many-body Monte–Carlo simulations have shown that temperature
 495 affects the weight and sharpness of the pair correlation peak, rather than shifting the peak to
 496 lower or higher momenta [61, 62].

497 4 Conclusions and Outlook

498 In summary, we have used the method of explicitly correlated Gaussians to study the exci-
 499 tations and pairing in two-dimensional trapped mesoscopic Fermi gases. For the closed-shell
 500 configuration of $3 + 3$ fermions, we reproduced the known [23, 26] non-monotonic depen-
 501 dence of the lowest monopole mode on the attractive interaction strength. For $1 + 1$, $2 + 2$,

502 and 3 + 3 fermions in the ground state, we found that time-reversed pairing is predominant
 503 at momenta significantly below the Fermi momentum. We explored the effects of varying the
 504 interaction strength (binding energy) and axial confinement (effective range) on the system
 505 properties. The difference between the experimental measurements for 6 + 6 fermions (where
 506 pairing mainly occurred at the Fermi surface) [24] and the calculations for 3 + 3 fermions is yet
 507 to be resolved. Improving the computational methodology to handle particle numbers greater
 508 than six — or conversely, obtaining the experimental data for fewer than twelve particles —
 509 would help to fill in this picture.

510 There are many avenues for future theoretical work on this topic. Means of increasing the
 511 numerical convergence rate for stronger binding energies, $\varepsilon_b > 2\hbar\omega_r$, (in addition to higher
 512 particle numbers) should continue to be sought. It would moreover be experimentally relevant
 513 to compare our (quasi-)two-dimensional calculation to a pure three-dimensional one and to
 514 confirm the effect of finite temperature in mesoscopic samples. Another extension would be
 515 to consider finite angular momentum sectors which become relevant in the case of anisotropic
 516 trapping potentials or spin imbalances. For instance, could one engineer a ‘few-body probe’
 517 of the Fermi–polaron problem [63]? Finally, in view of the large-scale quench experiments
 518 reported in Ref. [64], it would be useful to simulate the effect of an interaction quench in the
 519 few-body limit in order to shed further light on the dynamics of the emergence of superfluidity
 520 in two-component Fermi gases.

521 Acknowledgements

522 The authors would like to acknowledge helpful discussions with Jesper Levinsen, Meera Par-
 523 ish, Andy Martin, Alex Kerin, Mitchell Knight, Xia-Ji Liu, and Hui Hu. We furthermore thank
 524 Desmond (Xiangyu) Yin for writing the first iteration of the code for Hamiltonian diagonal-
 525 isation via the method of explicitly correlated Gaussians. This research was supported by the
 526 Australian Research Council Centre of Excellence in Future Low-Energy Electronics and Tech-
 527 nologies (FLEET, Project No. CE170100039) and funded by the Australian government. Emma
 528 Laird was supported by a Women-in-FLEET research fellowship.

529 A Method of Explicitly Correlated Gaussians

530 To numerically solve the time-independent Schrödinger equation for the Hamiltonian given by
 531 Eq. (1), we complement the stochastic variational method with the use of explicitly correlated
 532 Gaussian basis functions [36]. In this section, we provide a concise pedagogical discussion
 533 of the main components of this approach which apply to solving systems of trapped two-
 534 component fermions. Other works which have implemented this technique in the same context
 535 include Refs. [39–41, 65–67].

536 Due to the quadratic form of both the kinetic energy and the external potential energy, the
 537 Hamiltonian (1) can be separated into a centre-of-mass component and a relative component:
 538 $\mathcal{H} = \mathcal{H}_{\text{com}} + \mathcal{H}_{\text{rel}}$. We define a set of independent Jacobi co-ordinates $\mathbf{x} = (\mathbf{x}_1, \mathbf{x}_2, \dots, \mathbf{x}_N)^T$,
 539 where $\mathbf{x}_N = (\mathbf{r}_1 + \mathbf{r}_2 + \dots + \mathbf{r}_N)/N$ denotes the centre-of-mass position and $(\mathbf{x}_1, \mathbf{x}_2, \dots, \mathbf{x}_{N-1})^T$
 540 corresponds to relative motion degrees of freedom. The eigenfunctions of the centre-of-mass
 541 Hamiltonian are just the well known non-interacting states of the two-dimensional harmonic
 542 oscillator for a particle with mass $M = m_1 + m_2 + \dots + m_N$: $\mathcal{H}_{\text{com}}\Psi_{\text{com}}(\mathbf{x}_N) = \mathcal{E}_{\text{com}}\Psi_{\text{com}}(\mathbf{x}_N)$.
 543 Thus, it only remains to solve the Schrödinger equation for the relative motion: $\mathcal{H}_{\text{rel}}\Psi_{\text{rel}}(\mathbf{x}_1,$
 544 $\mathbf{x}_2, \dots, \mathbf{x}_{N-1}) = \mathcal{E}_{\text{rel}}\Psi_{\text{rel}}(\mathbf{x}_1, \mathbf{x}_2, \dots, \mathbf{x}_{N-1})$ [68].

545 The Jacobi vectors \mathbf{x} and single-particle co-ordinates $\mathbf{y} = (\mathbf{r}_1^\uparrow, \mathbf{r}_2^\downarrow, \mathbf{r}_3^\uparrow, \dots, \mathbf{r}_N^\downarrow)$ are related by
 546 an $N \times N$ linear transformation matrix \mathbb{U} [68]:

$$\mathbf{x} = \mathbb{U}\mathbf{y} \quad \longrightarrow \quad \mathbf{x}_i = \sum_{j=1}^N \mathbb{U}_{ij} \mathbf{r}_j^\sigma, \quad \mathbf{r}_i^\sigma = \sum_{j=1}^N (\mathbb{U}^{-1})_{ij} \mathbf{x}_j \quad (i = 1, \dots, N). \quad (\text{A.1})$$

547 Here, we have introduced a superscript on the single-particle co-ordinates to designate the
 548 pseudospin ($\sigma = \uparrow, \downarrow$) and have ordered them in such a way that the first atom is spin-up, the
 549 second is spin-down, the third is spin-up, and so forth. Note, in addition, that \mathbf{x} and \mathbf{y} are
 550 ‘supervectors’ (or vectors of vectors) and the double-line font is used in this work to signify a
 551 matrix. For two-component Fermi gases with balanced spins ($N = 2N_\uparrow = 2N_\downarrow$), we choose to
 552 construct \mathbb{U} in a manner following Ref. [41]: The first N_\uparrow Jacobi co-ordinates correspond to the
 553 distances between unlike pairs of fermions. The next $N_\uparrow/2$ [or $(N_\uparrow - 1)/2$ if N_\uparrow is odd] Jacobi
 554 co-ordinates correspond to the distances between the centres of mass of the first and second
 555 pair, the third and fourth pair, and so on. The remaining Jacobi vectors connect the larger sub-
 556 units. For example, in the case of $N = 6$ the transformation matrix is (with $m_{12\dots i} \equiv m_1 + m_2$
 557 $+ \dots + m_i$ and $m_{12\dots N} \equiv m_1 + m_2 + \dots + m_N = M$):

$$\mathbb{U} = \begin{pmatrix} 1 & -1 & 0 & 0 & 0 & 0 \\ 0 & 0 & 1 & -1 & 0 & 0 \\ 0 & 0 & 0 & 0 & 1 & -1 \\ m_1 \mathbf{r}_1^\uparrow / m_{12} & m_2 \mathbf{r}_2^\downarrow / m_{12} & -m_3 \mathbf{r}_3^\uparrow / m_{34} & -m_4 \mathbf{r}_4^\downarrow / m_{34} & 0 & 0 \\ m_1 \mathbf{r}_1^\uparrow / m_{1234} & m_2 \mathbf{r}_2^\downarrow / m_{1234} & m_3 \mathbf{r}_3^\uparrow / m_{1234} & m_4 \mathbf{r}_4^\downarrow / m_{1234} & -m_5 \mathbf{r}_5^\uparrow / m_{56} & -m_6 \mathbf{r}_6^\downarrow / m_{56} \\ m_1 \mathbf{r}_1^\uparrow / M & m_2 \mathbf{r}_2^\downarrow / M & m_3 \mathbf{r}_3^\uparrow / M & m_4 \mathbf{r}_4^\downarrow / M & m_5 \mathbf{r}_5^\uparrow / M & m_6 \mathbf{r}_6^\downarrow / M \end{pmatrix}. \quad (\text{A.2})$$

558 The relative Hamiltonian \mathcal{H}_{rel} may be recast in terms of the relative Jacobi co-ordinates \mathbf{x}
 559 $= (\mathbf{x}_1, \mathbf{x}_2, \dots, \mathbf{x}_{N-1})^T$ (in the remainder of this section *only*, the supervector \mathbf{x} excludes the
 560 centre-of-mass position) [68]. The relative kinetic energy operator T can be rewritten as

$$T = \sum_{i=1}^{N-1} -\frac{\hbar^2}{2\mu_i} \nabla_{\mathbf{x}_i}^2, \quad \mu_i = \left[\sum_{j=1}^N \frac{(\mathbb{U}_{ij})^2}{m_j} \right]^{-1}, \quad (\text{A.3})$$

561 where μ_i is the mass associated with the Jacobi co-ordinate \mathbf{x}_i . Similarly, the harmonic trapping
 562 potential term becomes

$$\sum_{i=1}^{N-1} \frac{\mu_i \omega_r^2}{2} \mathbf{x}_i^2, \quad (\text{A.4})$$

563 while the two-body interaction term is transformed by reformulating the interparticle distance
 564 vector:

$$\sum_{i=1}^N \sum_{j=i+1}^N V_{\text{int}}(r_{ij}), \quad r_{ij} \equiv |\mathbf{r}_i - \mathbf{r}_j| = [\boldsymbol{\omega}^{(ij)}]^T \mathbf{x}. \quad (\text{A.5})$$

565 Above, $\boldsymbol{\omega}$ is a transformation tensor whose (i, j) -th component is an $(N - 1)$ -dimensional
 566 vector with the p -th element given by $[\boldsymbol{\omega}^{(ij)}]_p = (\mathbb{U}^{-1})_{ip} - (\mathbb{U}^{-1})_{jp}$ [68].

567 We expand the eigenstates of the relative Hamiltonian in terms of explicitly correlated
 568 Gaussian basis functions. The unsymmetrised basis functions for states with zero total relative
 569 orbital angular momentum may be written as follows [68] using single-particle co-ordinates,

$$\phi_\alpha(\mathbf{y}) = \prod_{j>i=1}^N \exp \left[-\frac{1}{2\alpha_{ij}^2} (\mathbf{r}_i - \mathbf{r}_j)^2 \right] = \exp \left[-\sum_{j>i=1}^N \frac{1}{2\alpha_{ij}^2} (\mathbf{r}_i - \mathbf{r}_j)^2 \right], \quad (\text{A.6})$$

570 and using Jacobi co-ordinates,

$$\phi_{\mathbb{A}}(\mathbf{x}) = \exp\left(-\frac{1}{2}\mathbf{x}^T\mathbb{A}\mathbf{x}\right), \quad \mathbb{A}_{pq} = \sum_{i=1}^N \sum_{j=i+1}^N \frac{1}{\alpha_{ij}^2} [\boldsymbol{\omega}^{(ij)}]_p [\boldsymbol{\omega}^{(ij)}]_q. \quad (\text{A.7})$$

571 The $N(N-1)/2$ Gaussian widths α_{ij} are treated as non-linear variational parameters which
 572 are selected semi-stochastically and optimised by minimising the energy of the state of inter-
 573 est. Physically, small α_{ij} are required to describe contributions that occur at small interparticle
 574 separations r_{ij} , while large α_{ij} are needed to describe contributions occurring at large r_{ij} . Due
 575 to the principle of Pauli exclusion, interparticle distances are generally much longer when the
 576 atom indices i and j correspond to identical fermions, rather than to distinguishable fermions.
 577 Consequently, the α_{ij} parameters are generated randomly with one concession: those corre-
 578 sponding to same-spin fermions are restricted to be on the order of the radial harmonic trap
 579 length l_r , while those corresponding to different-spin fermions are permitted to range from a
 580 fraction of the interaction potential width r_0 up to a couple of times l_r [65]. Numerically, each
 581 basis function is encoded as a unique $(N-1) \times (N-1)$ correlation matrix \mathbb{A} , which has the
 582 properties of being real, symmetric and positive definite by virtue of the fact that the Gaussian
 583 widths are positive real numbers. The property of positive definiteness ensures that the basis
 584 functions are normalisable [68].

585 The correlated Gaussian technique relies on a generalisation of the variational principle
 586 which accounts for excited states [38]. The basic principle states that the expectation value
 587 of a Hamiltonian, say \mathcal{H}_{rel} , with respect to any normalised wave function provides an upper
 588 bound on the exact ground-state energy. If we now assume that $\varepsilon_1 \leq \varepsilon_2 \leq \dots$ are the exact
 589 eigenenergies of \mathcal{H}_{rel} , and $\mathcal{E}_1 \leq \mathcal{E}_2 \leq \dots \leq \mathcal{E}_{N_b}$ are the variational eigenvalues of \mathcal{H}_{rel} obtained
 590 from the subspace spanned by N_b basis functions — then the generalised principle informs us
 591 that $\varepsilon_1 \leq \mathcal{E}_1$, $\varepsilon_2 \leq \mathcal{E}_2$, \dots , $\varepsilon_{N_b} \leq \mathcal{E}_{N_b}$. This is proven in Sec. 3.1 of Ref. [68].

592 For the n^{th} eigenstate of \mathcal{H}_{rel} , the expansion in the correlated Gaussian basis (ignoring sym-
 593 metrisation for now) reads,

$$\Psi_{\text{rel}}^{(n)} = \sum_{i=1}^{N_b} c_i^{(n)} \phi_{\mathbb{A}_i}(\mathbf{x}), \quad (\text{A.8})$$

594 where the expansion coefficients $c_i^{(n)}$ are linear variational parameters. Minimising the varia-
 595 tional energy \mathcal{E}_n with respect to these coefficients leads to a generalised eigenvalue problem
 596 [38, 68]: $\mathbb{H}_{\text{rel}}\mathbb{C} = \mathbb{E}\mathbb{O}\mathbb{C}$. Here, \mathbb{H}_{rel} and \mathbb{O} are the Hamiltonian and overlap matrices, respec-
 597 tively, with elements given by (in two dimensions)

$$(\mathbb{H}_{\text{rel}})_{\mathbb{A}_i\mathbb{A}_j} \equiv \langle \phi_{\mathbb{A}_i} | \mathcal{H}_{\text{rel}} | \phi_{\mathbb{A}_j} \rangle, \quad \mathbb{O}_{\mathbb{A}_i\mathbb{A}_j} \equiv \langle \phi_{\mathbb{A}_i} | \phi_{\mathbb{A}_j} \rangle = \frac{(2\pi)^{N-1}}{\det[\mathbb{A}_i + \mathbb{A}_j]} \quad (i, j = 1, \dots, N_b). \quad (\text{A.9})$$

598 The n^{th} lowest variational eigenvalue \mathcal{E}_n corresponds to the n^{th} diagonal element of the diago-
 599 nal matrix \mathbb{E} , while the associated eigenvector $\mathbf{c}^{(n)}$ is contained in the n^{th} column of the matrix
 600 \mathbb{C} (not to be mistaken for the other \mathbb{C} matrix defined in Appendices D and E). The generalised
 601 variational principle guarantees that \mathcal{E}_n provides an upper bound on the n^{th} exact eigenenergy
 602 ε_n of \mathcal{H}_{rel} [38, 68].

603 Conveniently, evaluating the matrix elements of \mathcal{H}_{rel} amounts to performing simple matrix
 604 operations on \mathbb{A} [68]. In two dimensions the (unsymmetrised) matrix element for the relative
 605 kinetic energy operator reads,

$$\langle \phi_{\mathbb{A}_i} | T | \phi_{\mathbb{A}_j} \rangle = \hbar^2 \text{Tr}[\mathbb{A}_i (\mathbb{A}_i + \mathbb{A}_j)^{-1} \mathbb{A}_j \mathbb{M}], \quad (\text{A.10})$$

606 where \mathbb{M} is a diagonal mass matrix defined by $\mathbb{M}_{kk} = 1/\mu_k$. The matrix elements for arbitrary
607 one- and two-body operators are respectively given by

$$\langle \phi_{\mathbb{A}_i} | V(\mathbf{r}_k) | \phi_{\mathbb{A}_j} \rangle = \mathbb{O}_{\mathbb{A}_i \mathbb{A}_j} \frac{b_k}{2\pi} \int d^2\mathbf{r} V(\mathbf{r}) \exp\left(-\frac{1}{2} b_k r^2\right), \quad (\text{A.11a})$$

$$\langle \phi_{\mathbb{A}_i} | V(\mathbf{r}_k - \mathbf{r}_l) | \phi_{\mathbb{A}_j} \rangle = \mathbb{O}_{\mathbb{A}_i \mathbb{A}_j} \frac{b_{kl}}{2\pi} \int d^2\mathbf{r} V(\mathbf{r}) \exp\left(-\frac{1}{2} b_{kl} r^2\right), \quad (\text{A.11b})$$

608 with

$$\frac{1}{b_k} = [\boldsymbol{\omega}^{(k)}]^T (\mathbb{A}_i + \mathbb{A}_j)^{-1} \boldsymbol{\omega}^{(k)}, \quad [\boldsymbol{\omega}^{(k)}]_p = (U^{-1})_{kp}, \quad (\text{A.12a})$$

$$\frac{1}{b_{kl}} = [\boldsymbol{\omega}^{(kl)}]^T (\mathbb{A}_i + \mathbb{A}_j)^{-1} \boldsymbol{\omega}^{(kl)}, \quad (\text{A.12b})$$

609 which can be used to treat the confining and interaction potentials [68]. Note that in order to
610 endow the wave function with fermionic exchange symmetry, the antisymmetrisation operator
611 must be acted on the unsymmetrised basis states when calculating the Hamiltonian and overlap
612 matrix elements — and this is described in Appendix D.

613 We follow the two-step procedure detailed in Refs. [38, 41] to construct the explicitly cor-
614 related Gaussian basis. The first step is the basis set *enlargement*, in which new basis functions
615 (new matrices \mathbb{A}_i) are added one at a time. The second step is the basis function *refinement*, in
616 which the existing \mathbb{A}_i matrices are adjusted one at a time. Both steps are cyclically repeated as
617 necessary until the energy of the state of interest is converged (changes by less than a preset,
618 very small value). Due to the fact that the basis is over-complete, the rate of convergence is
619 rapid [36].

620 To add a new basis function \mathbb{A}_i to the basis set, we generate a large number (say ‘ p ’) of trial
621 basis functions stochastically within preset parameter windows: $\{\mathbb{A}_{i,1}, \mathbb{A}_{i,2}, \dots, \mathbb{A}_{i,p}\}$. Since
622 one more basis state always lowers the energy¹⁰, we choose to keep the matrix $\mathbb{A}_{i,j} \equiv \mathbb{A}_i$ that
623 lowers the energy of the state of interest the most. Similarly, to refine an existing basis function
624 \mathbb{A}_i , we generate ‘ p ’ trial replacement basis functions stochastically: $\{\mathbb{A}'_{i,1}, \mathbb{A}'_{i,2}, \dots, \mathbb{A}'_{i,p}\}$. We
625 subsequently determine which one affords the lowest energy for the state of interest, labelling
626 it by $\mathbb{A}'_{i,j} \equiv \mathbb{A}'_i$, and if this energy is lower than the original energy, then we replace \mathbb{A}_i by \mathbb{A}'_i .

627 In both the enlargement and refinement phases, in order to determine how the energy
628 eigenvalues are affected by the inclusion of a given trial basis function, we do not need to
629 solve the full $(K+1) \times (K+1)$ -dimensional generalised eigenvalue problem through matrix
630 diagonalisation. Instead, we can exclude the concerned (i^{th}) row and column from the Hamil-
631 tonian and overlap matrices, and diagonalise the resulting generalised eigenvalue problem
632 of size $K \times K$. The eigenvalues of the $(K+1)$ -dimensional matrix can then be found as the
633 roots of a secular equation which depends on the eigenvalues and normalised eigenvectors of
634 the K -dimensional submatrix, and on the i^{th} row and column of \mathbb{H}_{rel} and \mathbb{O} . The full details
635 — which are based on Gram–Schmidt orthogonalisation¹¹ — are provided in Ref. [32]. Se-
636 lecting from a large number of trial basis functions thus becomes numerically feasible since
637 root-finding is computationally much faster than matrix diagonalisation, and because the K -
638 dimensional submatrix need only be diagonalised once. In addition, both the enlargement
639 and refinement subroutines can be efficiently parallelised over a number (N_c) of MPI cores
640 on a high-performance computer [38]. We generate p/N_c trial basis functions on each core,
641 and then compare the eigenenergies across all N_c cores by using the ‘MPI_Allreduce’ function.

¹⁰If a basis of size K yields an ordered set of eigenvalues $\lambda_1 \leq \lambda_2 \leq \dots \leq \lambda_K$, then a basis of size $K+1$ will yield an ordered set of eigenvalues $\gamma_1 \leq \gamma_2 \leq \dots \leq \gamma_{K+1}$, such that $\gamma_1 \leq \lambda_1 \leq \gamma_2 \leq \lambda_2 \leq \dots \leq \gamma_K \leq \lambda_K \leq \gamma_{K+1}$.

¹¹This orthogonalisation technique avoids numerical instabilities caused by linear dependencies which may otherwise arise due to the over-completeness of the basis set.

642 Once the basis function that lowers the energy the most has been chosen, this information is
 643 synchronised across all cores by using the ‘MPI_Bcast’ function.

644 The results for 1 + 1, 2 + 2, and 3 + 3 fermions are shown in Sec. 3. The main hindrance to
 645 theoretically considering higher particle numbers derives from the first-quantised formulation
 646 of the ECG method — namely, the antisymmetrisation requirement to sum over all possible
 647 permutations of identical particles, as mentioned above and in Appendix D. For equally popu-
 648 lated two-component systems of N fermions, this number of permutations is $N_p = [(N/2)!]^2$,
 649 such that the evaluation of a single matrix element becomes *very* time consuming as the num-
 650 ber of particles increases (refer to Table 1). Combined with basis sizes on the order of at least
 651 thousands of states, this makes the 6 + 6 system of fermions considered by experiment [24]
 computationally out of reach.

N	2	4	6	8	10	12
N_p	1	4	36	576	14,400	518,400

Table 1: Scaling of the number of permutations N_p with the number of particles N .

652

653 B Comparison to a Contact Interaction

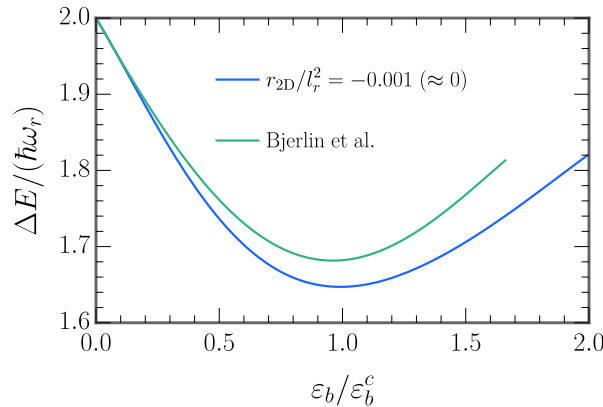


Figure 7: The lowest monopole excitation spectrum for $N_\uparrow + N_\downarrow = 3 + 3$ fermions. We overlay our result at zero effective range (in blue) on the contact interaction result from Fig. 1 of Ref. [26] (in green). In each case, we normalise ε_b by a critical value ε_b^c , which is defined as the two-body binding energy that gives the minimum excitation energy ΔE .

654 The spatial extent of the potential selected to model short-range binary collisions in the ul-
 655 tracold Fermi gas can, to a small degree, quantitatively affect the lowest monopole excitation
 656 spectrum. Above in Fig. 7, we show again our result for 3 + 3 fermions at an effective range
 657 of $r_{2D}/l_r^2 = -0.001 \approx 0$, which we obtained by using the finite-range Gaussian interaction po-
 658 tential given in Eq. (3). Although the effective range of this potential is fixed and close to zero,
 659 the physical width r_0 varies between $0.01l_r$ and $0.05l_r$ over the depicted range of binding en-
 660 ergies. This leads to a small downward shift in the excitation energy — which becomes larger
 661 with increasing binding energy — when compared to an analogous calculation [26] based on
 662 a contact interaction with zero range ($r_0 \rightarrow 0$) [69, 70]. Within our model, we can estimate
 663 the zero-range limit of a contact interaction by starting with the value of ΔE at a particular

664 binding energy ε_b , and then systematically reducing the Gaussian width r_0 , while varying the
 665 depth V_0 such that ε_b remains constant. In this way, we can construct a plot of ΔE versus r_0
 666 and then extrapolate to the limit of $r_0 = 0$ [41]. The process can subsequently be repeated
 667 at all desired binding energies. Interestingly, due to the second term in Eq. (3), decreasing
 668 the potential width for a fixed binding energy and basis size causes ΔE to *increase*. However,
 669 since this also corresponds to a deeper potential, the result becomes less accurate. Increasing
 670 the basis size to improve the level of accuracy, in turn, lowers ΔE . In general, we found that
 671 the very deep and narrow potentials generated by this limiting procedure made it necessary
 672 to use very large basis sets in order to numerically converge the excitation energy. Therefore,
 673 we only performed this check at a single binding energy.

674 C Definitions of the Pair Correlator and Density Matrices

675 As done in Eq. (7), we define the second-order pair correlation function for opposing spins as
 676 follows:

$$\mathcal{C}^{(2)}(\mathbf{p}_1, \mathbf{p}_2) = \langle n_\uparrow(\mathbf{p}_1) n_\downarrow(\mathbf{p}_2) \rangle - \langle n_\uparrow(\mathbf{p}_1) \rangle \langle n_\downarrow(\mathbf{p}_2) \rangle, \quad (\text{C.1})$$

677 where

$$\tilde{\rho}(\mathbf{p}_1, \mathbf{p}_2) \equiv \langle n_\uparrow(\mathbf{p}_1) n_\downarrow(\mathbf{p}_2) \rangle = \langle c_{\mathbf{p}_1\uparrow}^\dagger c_{\mathbf{p}_1\uparrow} c_{\mathbf{p}_2\downarrow}^\dagger c_{\mathbf{p}_2\downarrow} \rangle, \quad (\text{C.2})$$

$$\tilde{\rho}_\uparrow(\mathbf{p}_1) \equiv \langle n_\uparrow(\mathbf{p}_1) \rangle = \langle c_{\mathbf{p}_1\uparrow}^\dagger c_{\mathbf{p}_1\uparrow} \rangle, \quad (\text{C.3})$$

$$\tilde{\rho}_\downarrow(\mathbf{p}_2) \equiv \langle n_\downarrow(\mathbf{p}_2) \rangle = \langle c_{\mathbf{p}_2\downarrow}^\dagger c_{\mathbf{p}_2\downarrow} \rangle. \quad (\text{C.4})$$

678 Here, $c_{\mathbf{p}\sigma}^\dagger$ ($c_{\mathbf{p}\sigma}$) is the fermionic creation (annihilation) operator for a particle with momentum
 679 \mathbf{p} and pseudospin σ in the language of second quantisation (with $\sigma = \uparrow, \downarrow$). The “ $\tilde{\rho}$ ” de-
 680 note momentum-space density matrix elements and these can be related to the position-space
 681 density matrix elements which we have calculated in the correlated Gaussian basis (refer to
 682 Appendices D and E, below).

683 To this end, we make use of the relationship between the creation operators in position
 684 $[\psi_\sigma^\dagger(\mathbf{r})]$ and momentum ($c_{\mathbf{p}\sigma}^\dagger$) space:

$$c_{\mathbf{p}\sigma}^\dagger = \frac{1}{2\pi} \int d\mathbf{r} \psi_\sigma^\dagger(\mathbf{r}) e^{i\mathbf{p}\cdot\mathbf{r}}, \quad (\text{C.5})$$

$$c_{\mathbf{p}\sigma} = \frac{1}{2\pi} \int d\mathbf{r} \psi_\sigma(\mathbf{r}) e^{-i\mathbf{p}\cdot\mathbf{r}}. \quad (\text{C.6})$$

685 Inserting these relations into the definition (C.3) of the one-body density matrix for the spin- \uparrow
 686 atoms in momentum space yields

$$\tilde{\rho}_\uparrow(\mathbf{p}_1) = \frac{1}{(2\pi)^2} \iint d\mathbf{r} d\mathbf{r}' \langle \psi_\uparrow^\dagger(\mathbf{r}) \psi_\uparrow(\mathbf{r}') \rangle e^{-i\mathbf{p}_1\cdot(\mathbf{r}'-\mathbf{r})} = \frac{1}{(2\pi)^2} \iint d\mathbf{r} d\mathbf{r}' \rho_\uparrow(\mathbf{r}, \mathbf{r}') e^{-i\mathbf{p}_1\cdot(\mathbf{r}'-\mathbf{r})}. \quad (\text{C.7})$$

687 This result involves the position-space one-body density matrix for the spin- \uparrow atoms, which
 688 can be written as

$$\rho_\uparrow(\mathbf{r}, \mathbf{r}') = \left[\int \cdots \int d\mathbf{r}_1^\uparrow d\mathbf{r}_2^\downarrow \cdots d\mathbf{r}_{N-1}^\uparrow d\mathbf{r}_N^\downarrow \left| \Psi(\mathbf{r}_1^\uparrow, \mathbf{r}_2^\downarrow, \cdots, \mathbf{r}_{N-1}^\uparrow, \mathbf{r}_N^\downarrow) \right|^2 \right]^{-1} \times$$

$$\int \cdots \int d\mathbf{r}_2^\downarrow d\mathbf{r}_3^\uparrow d\mathbf{r}_4^\downarrow \cdots d\mathbf{r}_{N-1}^\uparrow d\mathbf{r}_N^\downarrow \Psi(\mathbf{r}, \mathbf{r}_2^\downarrow, \mathbf{r}_3^\uparrow, \mathbf{r}_4^\downarrow, \cdots, \mathbf{r}_{N-1}^\uparrow, \mathbf{r}_N^\downarrow) \Psi^*(\mathbf{r}', \mathbf{r}_2^\downarrow, \mathbf{r}_3^\uparrow, \mathbf{r}_4^\downarrow, \cdots, \mathbf{r}_{N-1}^\uparrow, \mathbf{r}_N^\downarrow) \quad (\text{C.8})$$

689 in the first quantisation picture, where $\Psi = \Psi_{\text{com}} \Psi_{\text{rel}}$ is the total N -body wave function. The
 690 first line of Eq. (C.8) is a normalisation constant; in the second line we integrate the density
 691 $\Psi \Psi^*$ over all co-ordinates except those of a single spin- \uparrow particle. Expressions analogous to
 692 Eqs. (C.7)–(C.8) can readily be written down for the spin- \downarrow case (C.4). Similarly, the two-body
 693 density matrix for spin- \uparrow -spin- \downarrow pairs is given by

$$\begin{aligned} \tilde{\rho}(\mathbf{p}_1, \mathbf{p}_2) &= \frac{1}{(2\pi)^4} \int \cdots \int d\mathbf{r}_1 d\mathbf{r}'_1 d\mathbf{r}_2 d\mathbf{r}'_2 \langle \psi_\uparrow^\dagger(\mathbf{r}_1) \psi_\uparrow(\mathbf{r}'_1) \psi_\downarrow^\dagger(\mathbf{r}_2) \psi_\downarrow(\mathbf{r}'_2) \rangle e^{-i\mathbf{p}_1 \cdot (\mathbf{r}'_1 - \mathbf{r}_1)} e^{-i\mathbf{p}_2 \cdot (\mathbf{r}'_2 - \mathbf{r}_2)} \\ &= \frac{1}{(2\pi)^4} \int \cdots \int d\mathbf{r}_1 d\mathbf{r}'_1 d\mathbf{r}_2 d\mathbf{r}'_2 \rho(\mathbf{r}_1, \mathbf{r}'_1; \mathbf{r}_2, \mathbf{r}'_2) e^{-i\mathbf{p}_1 \cdot (\mathbf{r}'_1 - \mathbf{r}_1)} e^{-i\mathbf{p}_2 \cdot (\mathbf{r}'_2 - \mathbf{r}_2)} \end{aligned} \quad (\text{C.9})$$

694 in momentum space, and by

$$\begin{aligned} \rho(\mathbf{r}_1, \mathbf{r}'_1; \mathbf{r}_2, \mathbf{r}'_2) &= \left[\int \cdots \int d\mathbf{r}_1^\uparrow d\mathbf{r}_2^\downarrow \cdots d\mathbf{r}_{N-1}^\uparrow d\mathbf{r}_N^\downarrow \left| \Psi(\mathbf{r}_1^\uparrow, \mathbf{r}_2^\downarrow, \cdots, \mathbf{r}_{N-1}^\uparrow, \mathbf{r}_N^\downarrow) \right|^2 \right]^{-1} \times \\ &\int \cdots \int d\mathbf{r}_3^\uparrow d\mathbf{r}_4^\downarrow \cdots d\mathbf{r}_{N-1}^\uparrow d\mathbf{r}_N^\downarrow \Psi(\mathbf{r}_1, \mathbf{r}_2, \mathbf{r}_3^\uparrow, \mathbf{r}_4^\downarrow, \cdots, \mathbf{r}_{N-1}^\uparrow, \mathbf{r}_N^\downarrow) \Psi^*(\mathbf{r}'_1, \mathbf{r}'_2, \mathbf{r}_3^\uparrow, \mathbf{r}_4^\downarrow, \cdots, \mathbf{r}_{N-1}^\uparrow, \mathbf{r}_N^\downarrow) \end{aligned} \quad (\text{C.10})$$

695 in position space. Above, we integrate over all co-ordinates except those of one spin- \uparrow particle
 696 and one spin- \downarrow particle. Note that all integrals in this section are two-dimensional, i.e, we have
 697 written $d\mathbf{r} \equiv d^2\mathbf{r}$ for brevity. Furthermore, for numerical convenience we order the atoms so
 698 that the first one is spin- \uparrow , the second is spin- \downarrow , the third is spin- \uparrow , etc., as done in Appendix A
 699 [see Eqs. (A.1)–(A.2)].

700 D Derivation of the One-Body Terms in the Pair Correlator

701 To derive closed analytical expressions for the one-body terms in Eq. (C.1), we follow the
 702 prescription given in Appendix A of Ref. [39] (which is in three dimensions), while making
 703 the necessary modifications for a two-dimensional system.

704 When we calculated the excitation spectra in Fig. 2, we separated off the centre-of-mass
 705 degrees of freedom and expanded the eigenstates of the relative Hamiltonian in terms of the
 706 explicitly correlated Gaussian basis functions. These basis functions depended on a set of non-
 707 linear variational parameters which were optimised through energy minimisation. In order
 708 to calculate the pair correlator $C^{(2)}$ we now need to utilise the full N -body wave function, so
 709 we multiply the optimised basis set by the unnormalised ground-state centre-of-mass wave
 710 function [39]:

$$\Psi_{\text{com}}^{(\text{GS})}(\mathbf{x}_N) = \exp\left(-\frac{\mathbf{x}_N^2}{2a_{\text{ho}}^2/N}\right), \quad \mathbf{x}_N = \sum_{i=1}^N \frac{\mathbf{r}_i^\sigma}{N}. \quad (\text{D.1})$$

711 The unsymmetrised (and unnormalised) basis functions that incorporate the centre-of-mass
 712 motion thus read as follows:

$$\phi_{\mathbb{A}}(\mathbf{x}) = \exp\left(-\frac{1}{2} \mathbf{x}^T \mathbb{A} \mathbf{x}\right), \quad (\text{D.2})$$

713 where $\mathbf{x} = (\mathbf{x}_1, \mathbf{x}_2, \dots, \mathbf{x}_{N-1}, \mathbf{x}_N)$ denotes the *full* set of N Jacobi position vectors defined in
 714 Appendix A. Here, \mathbb{A} is an $N \times N$ symmetric and positive definite correlation matrix comprising
 715 $N(N-1)/2$ variational parameters (the \mathbb{A}_{ij} with $i = 1, \dots, N-1$ and $j \geq i$), which are
 716 optimised semi-stochastically. To force the centre-of-mass degrees of freedom into the ground
 717 state, we manually set the matrix elements \mathbb{A}_{iN} and \mathbb{A}_{Ni} (with $i = 1, \dots, N-1$) to zero, while
 718 setting \mathbb{A}_{NN} to N/a_{ho}^2 [39]. We reiterate that \mathbf{x} is a ‘supervector’ (or vector of vectors) and the
 719 double-line font is used in this work to designate a matrix. The Jacobi vectors \mathbf{x} and single-
 720 particle co-ordinates $\mathbf{y} \equiv (\mathbf{y}_1, \dots, \mathbf{y}_N) = (\mathbf{r}_1^\uparrow, \mathbf{r}_2^\downarrow, \mathbf{r}_3^\uparrow, \dots, \mathbf{r}_N^\downarrow)$ are related by the $N \times N$ linear
 721 transformation matrix \mathbb{U} , which has been defined in Eqs. (A.1)–(A.2) of Appendix A.

722 Now that we have set up the system, our first goal is to derive the correlated Gaussian
 723 matrix elements of the real-space one-body density matrix for the spin- \uparrow atoms, Eq. (C.8) (the
 724 derivation for the spin- \downarrow atoms follows analogously):

$$\begin{aligned} \frac{[\rho_\uparrow(\mathbf{r}, \mathbf{r}')]_{\mathbb{A}\mathbb{A}'}}{\mathbb{O}_{\mathbb{A}\mathbb{A}'}} &\equiv \frac{\langle \phi_{\mathbb{A}} | \rho_\uparrow | \phi_{\mathbb{A}'} \rangle}{\langle \phi_{\mathbb{A}} | \phi_{\mathbb{A}'} \rangle} \\ &= (\mathbb{O}_{\mathbb{A}\mathbb{A}'})^{-1} \int \dots \int d^{2N-2} \mathbf{y}_{\text{red}} \left[\int d^2 \mathbf{r}_1^\uparrow \delta(\mathbf{r} - \mathbf{r}_1^\uparrow) \phi_{\mathbb{A}}(\mathbf{x}) \right] \left[\int d^2 \mathbf{r}_1^\uparrow \delta(\mathbf{r}' - \mathbf{r}_1^\uparrow) \phi_{\mathbb{A}'}(\mathbf{x}) \right]. \end{aligned} \quad (\text{D.3})$$

725 In this equation we have defined $\mathbf{y}_{\text{red}} = (\mathbf{r}_2^\downarrow, \mathbf{r}_3^\uparrow, \mathbf{r}_4^\downarrow, \dots, \mathbf{r}_{N-1}^\uparrow, \mathbf{r}_N^\downarrow)$, $\delta(\dots)$ represents the two-
 726 dimensional Dirac delta function, and

$$\mathbb{O}_{\mathbb{A}\mathbb{A}'} \equiv \langle \phi_{\mathbb{A}} | \phi_{\mathbb{A}'} \rangle = \frac{(2\pi)^N}{\det[\mathbb{A} + \mathbb{A}']} \quad (\text{D.4})$$

727 is the overlap matrix element [68] for the (unsymmetrised) ECG basis functions associated
 728 with the correlation matrices \mathbb{A} and \mathbb{A}' . It is convenient to express the right-hand-side of Eq.
 729 (D.3) in terms of the Gaussian generating function [68],

$$g(\mathbf{s}; \mathbb{A}, \mathbf{x}) = \exp\left(-\frac{1}{2} \mathbf{x}^T \mathbb{A} \mathbf{x} + \mathbf{s}^T \mathbf{x}\right), \quad (\text{D.5})$$

730 where \mathbf{s} denotes an auxiliary supervector with the same dimensionality as \mathbf{x} . The basis func-
 731 tion in Eq. (D.2) can therefore be written as $\phi_{\mathbb{A}}(\mathbf{x}) = g(\mathbf{0}; \mathbb{A}, \mathbf{x})$. By using the fact that $\mathbf{x}^T \mathbb{A} \mathbf{x} =$
 732 $\mathbf{y}^T \mathbb{U}^T \mathbb{A} \mathbb{U} \mathbf{y}$, we re-express the basis function $\phi_{\mathbb{A}}$ in terms of \mathbf{y} and separate off the \mathbf{r}_1^\uparrow depen-
 733 dence:

$$\phi_{\mathbb{A}}(\mathbf{y}) = g(\mathbf{0}; \mathbb{B}, \mathbf{y}_{\text{red}}) \exp\left[-\frac{1}{2} b_1 (\mathbf{r}_1^\uparrow)^2 - (\mathbf{b}^T \mathbf{y}_{\text{red}})^T \mathbf{r}_1^\uparrow\right]. \quad (\text{D.6})$$

734 Here, \mathbb{B} is an $(N-1) \times (N-1)$ -dimensional matrix given by $\mathbb{U}^T \mathbb{A} \mathbb{U}$ with the first row and column
 735 removed, \mathbf{b} is an $(N-1)$ -dimensional vector given by $((\mathbb{U}^T \mathbb{A} \mathbb{U})_{12}, \dots, (\mathbb{U}^T \mathbb{A} \mathbb{U})_{1N})$, and b_1 is a
 736 scalar given by $(\mathbb{U}^T \mathbb{A} \mathbb{U})_{11}$. In addition, Eq. (D.6) contains the quantity

$$(\mathbf{b}^T \mathbf{y}_{\text{red}})^T \mathbf{r}_1^\uparrow = \sum_{j=2}^N \mathbf{b}_{j-1} \mathbf{y}_j^T \mathbf{r}_1^\uparrow, \quad (\text{D.7})$$

737 where \mathbf{b}_j denotes the j^{th} element of the vector \mathbf{b} . To continue we define $\{\mathbb{B}', \mathbf{b}', b'_1\}$ analo-
 738 gously to $\{\mathbb{B}, \mathbf{b}, b_1\}$, substitute the expressions for $\phi_{\mathbb{A}}(\mathbf{x}) \rightarrow \phi_{\mathbb{A}}(\mathbf{y})$ and $\phi_{\mathbb{A}'}(\mathbf{x}) \rightarrow \phi_{\mathbb{A}'}(\mathbf{y})$ into
 739 Eq. (D.3), and then evaluate the two Dirac delta functions. This yields

$$[\rho_\uparrow(\mathbf{r}, \mathbf{r}')]_{\mathbb{A}\mathbb{A}'} \equiv \langle \phi_{\mathbb{A}} | \rho_\uparrow | \phi_{\mathbb{A}'} \rangle = \int \dots \int d^{2N-2} \mathbf{y}_{\text{red}} g(\mathbf{0}; \mathbb{B}, \mathbf{y}_{\text{red}}) g(\mathbf{0}; \mathbb{B}', \mathbf{y}_{\text{red}}) \times$$

$$\exp\left\{-\frac{1}{2}b_1\mathbf{r}^2 - \frac{1}{2}b'_1(\mathbf{r}')^2 - (\mathbf{b}^T\mathbf{y}_{\text{red}})^T\mathbf{r} - [(\mathbf{b}')^T\mathbf{y}_{\text{red}}]^T\mathbf{r}'\right\}, \quad (\text{D.8})$$

740 which can be rewritten as

$$[\rho_{\uparrow}(\mathbf{r}, \mathbf{r}')]_{\mathbb{A}\mathbb{A}'} = \int \cdots \int d^{2N-2}\mathbf{y}_{\text{red}} g[-(\mathbf{b}\mathbf{r} + \mathbf{b}'\mathbf{r}'); \mathbb{B} + \mathbb{B}', \mathbf{y}_{\text{red}}] \exp\left\{-\frac{1}{2}[b_1\mathbf{r}^2 + b'_1(\mathbf{r}')^2]\right\}. \quad (\text{D.9})$$

741 Above, the quantity $\mathbf{b}\mathbf{r}$ is an $(N-1)$ -dimensional supervector with elements $\mathbf{b}_j\mathbf{r}$, where $j = 1,$
742 $\dots, N-1$. By employing the two-dimensional relation [68] shown below,

$$\int \cdots \int d^{2N}\mathbf{x} g(\mathbf{s}; \mathbb{A}, \mathbf{x}) = \frac{(2\pi)^N}{\det[\mathbb{A}]} \exp\left(\frac{1}{2}\mathbf{s}^T\mathbb{A}^{-1}\mathbf{s}\right), \quad (\text{D.10})$$

743 we arrive at a compact expression for the correlated Gaussian matrix elements of the one-body
744 density matrix in real space:

$$[\rho_{\uparrow}(\mathbf{r}, \mathbf{r}')]_{\mathbb{A}\mathbb{A}'} = c_1 \exp\left\{-\frac{1}{2}[c\mathbf{r}^2 + c'(\mathbf{r}')^2 - a\mathbf{r}^T\mathbf{r}']\right\}, \quad (\text{D.11})$$

745 which depends on the following scalars,

$$c_1 = \frac{(2\pi)^{N-1}}{\det[\mathbb{B} + \mathbb{B}']}, \quad (\text{D.12})$$

$$c = b_1 - \mathbf{b}^T\mathbb{C}\mathbf{b}, \quad (\text{D.13})$$

$$c' = b'_1 - (\mathbf{b}')^T\mathbb{C}\mathbf{b}', \quad (\text{D.14})$$

$$a = \mathbf{b}^T\mathbb{C}\mathbf{b}' + (\mathbf{b}')^T\mathbb{C}\mathbf{b}, \quad (\text{D.15})$$

746 and on the matrix,

$$\mathbb{C} = (\mathbb{B} + \mathbb{B}')^{-1}. \quad (\text{D.16})$$

747 Our second goal is now to evaluate the Fourier transform of Eq. (D.11) — as defined by
748 Eq. (C.7) — in order to obtain the correlated Gaussian matrix elements of the one-body density
749 matrix in momentum space:

$$[\tilde{\rho}_{\uparrow}(\mathbf{p}_1)]_{\mathbb{A}\mathbb{A}'} = \frac{1}{(2\pi)^2} \int \int d^2\mathbf{r} d^2\mathbf{r}' [\rho_{\uparrow}(\mathbf{r}, \mathbf{r}')]_{\mathbb{A}\mathbb{A}'} e^{-i\mathbf{p}_1 \cdot (\mathbf{r}' - \mathbf{r})}. \quad (\text{D.17})$$

750 By defining $\mathbf{X} = \mathbf{r}' - \mathbf{r}$, Eq. (D.17) becomes

$$[\tilde{\rho}_{\uparrow}(\mathbf{p}_1)]_{\mathbb{A}\mathbb{A}'} = \frac{c_1}{(2\pi)^2} \int \int d^2\mathbf{r} d^2\mathbf{X} \exp[-i(p_1^x X_x + p_1^y X_y)] \times \exp\left\{\frac{1}{2}[g_1(r_x^2 + r_y^2) + g_2(X_x^2 + X_y^2) + g_3(r_x X_x + r_y X_y)]\right\}, \quad (\text{D.18})$$

751 with the scalars,

$$g_1 = a - c - c', \quad (\text{D.19})$$

$$g_2 = -c', \quad (\text{D.20})$$

$$g_3 = a - 2c'. \quad (\text{D.21})$$

752 For $g_1 < 0$, the integral over \mathbf{r} can be performed analytically:

$$\begin{aligned} & \int_{-\infty}^{+\infty} \int_{-\infty}^{+\infty} dr_x dr_y \exp \left\{ \frac{1}{2} \left[g_1 (r_x^2 + r_y^2) + g_2 (X_x^2 + X_y^2) + g_3 (r_x X_x + r_y X_y) \right] \right\} \\ &= -\frac{2\pi}{g_1} \exp \left[\frac{4g_1 g_2 - g_3^2}{8g_1} (X_x^2 + X_y^2) \right]. \end{aligned} \quad (\text{D.22})$$

753 This allows the integral over \mathbf{X} to then be carried out analytically, as well, for $4g_1 g_2 - g_3^2 > 0$:

$$\begin{aligned} & \int_{-\infty}^{+\infty} \int_{-\infty}^{+\infty} dX_x dX_y \exp[-i(p_1^x X_x + p_1^y X_y)] \left\{ -\frac{2\pi}{g_1} \exp \left[\frac{4g_1 g_2 - g_3^2}{8g_1} (X_x^2 + X_y^2) \right] \right\} \\ &= \frac{16\pi^2}{4g_1 g_2 - g_3^2} \exp \left\{ \frac{2g_1}{4g_1 g_2 - g_3^2} [(p_1^x)^2 + (p_1^y)^2] \right\}. \end{aligned} \quad (\text{D.23})$$

754 Thus, the correlated Gaussian matrix elements of the momentum-space one-body density ma-
755 trix for the spin- \uparrow atoms are given by

$$[\tilde{\rho}_\uparrow(\mathbf{p}_1)]_{\mathbb{A}\mathbb{A}'} = \frac{4c_1}{4g_1 g_2 - g_3^2} \exp \left(\frac{2g_1}{4g_1 g_2 - g_3^2} p_1^2 \right), \quad (\text{D.24})$$

756 with momentum $p_1 \equiv |\mathbf{p}_1|$. We have checked that the two conditions, $g_1 < 0$ and $4g_1 g_2 - g_3^2$
757 > 0 , are indeed satisfied numerically. We can now evaluate Eq. (C.3) for the ground state (GS)
758 by using the derived results for $[\tilde{\rho}_\uparrow(\mathbf{p}_1)]_{\mathbb{A}_i \mathbb{A}_j}$ (D.24) and $\mathbb{O}_{\mathbb{A}_i \mathbb{A}_j}$ (D.4):

$$\langle n_\uparrow(\mathbf{p}_1) \rangle \equiv \frac{\langle \Psi^{(\text{GS})} | n_\uparrow(\mathbf{p}_1) | \Psi^{(\text{GS})} \rangle}{\langle \Psi^{(\text{GS})} | \Psi^{(\text{GS})} \rangle} = \frac{\sum_{i,j} c_i^* [\tilde{\rho}_\uparrow(\mathbf{p}_1)]_{\mathbb{A}_i \mathbb{A}_j} c_j}{\sum_{i,j} c_i^* \mathbb{O}_{\mathbb{A}_i \mathbb{A}_j} c_j}. \quad (\text{D.25})$$

759 Above, the second expression is obtained from the first by inserting two complete sets of ECG
760 basis states into both the numerator and denominator, and $c_i = \langle \phi_{\mathbb{A}_i} | \Psi^{(\text{GS})} \rangle$ is the i^{th} (real)
761 coefficient of the full ground-state wave function which is found by diagonalising the Hamil-
762 tonian (see Appendix A).

763 To enhance the clarity of our discussion up until this point, we have used unsymmetrised
764 basis functions — but of course, in reality, when we derive the ECG matrix elements we need
765 to appropriately *antisymmetrise* the fermionic basis [68]. This means that we need to act the
766 antisymmetrisation operator,

$$\mathcal{P} = \sum_{i=1}^{N_p} s_i P_i, \quad (\text{D.26})$$

767 on both the bra $\langle \phi_{\mathbb{A}} |$ and the ket $|\phi_{\mathbb{A}'} \rangle$. Here, \mathcal{P} represents the sum of all possible N_p permu-
768 tation operators P_i for the reordering of identical fermions, weighted by the signs s_i of those
769 permutations. Conveniently, in the ECG approach acting a single permutation operator on a
770 basis function simply amounts to a redefinition of the correlation matrix $\mathbb{A} \rightarrow \bar{\mathbb{A}}(i)$:

$$P_i \phi_{\mathbb{A}}(\mathbf{x}) = P_i \exp \left(-\frac{1}{2} \mathbf{x}^T \mathbb{A} \mathbf{x} \right) = \exp \left\{ -\frac{1}{2} \mathbf{x}^T \left[(\mathbb{T}_{P_i})^T \mathbb{A} \mathbb{T}_{P_i} \right] \mathbf{x} \right\} \equiv \exp \left[-\frac{1}{2} \mathbf{x}^T \bar{\mathbb{A}}(i) \mathbf{x} \right] = \phi_{\bar{\mathbb{A}}(i)}(\mathbf{x}), \quad (\text{D.27})$$

771 where \mathbb{T}_{P_i} is the $(N-1) \times (N-1)$ -dimensional permutation matrix corresponding to the i^{th}
772 permutation — as defined in Eq. (2.30) of Ref. [68]. Accordingly, it is straightforward to write
773 down the antisymmetrised matrix element of a given operator, say \mathcal{B} :

$$\langle \phi_{\mathbb{A}} | \mathcal{B} | \phi_{\mathbb{A}'} \rangle \rightarrow \langle \mathcal{P} \phi_{\mathbb{A}} | \mathcal{B} | \mathcal{P} \phi_{\mathbb{A}'} \rangle = \sum_{i=1}^{N_p} \sum_{j=1}^{N_p} s_i s_j \langle \phi_{\bar{\mathbb{A}}(i)} | \mathcal{B} | \phi_{\bar{\mathbb{A}}'(j)} \rangle, \quad (\text{D.28})$$

774 which comprises N_p^2 terms. If \mathcal{B} is invariant under the exchange of any pair of identical atoms
 775 (i.e., if it commutes with all permutation operators P_i), then we can use this fact — and also
 776 the fact that each permutation is an idempotent operator, $(P_i)^2 = 1 \forall i$ — to show that

$$\langle \mathcal{P}\phi_{\mathbb{A}} | \mathcal{B} | \mathcal{P}\phi_{\mathbb{A}'} \rangle = N_p \langle \mathcal{P}\phi_{\mathbb{A}} | \mathcal{B} | \phi_{\mathbb{A}'} \rangle = N_p \langle \phi_{\mathbb{A}} | \mathcal{B} | \mathcal{P}\phi_{\mathbb{A}'} \rangle. \quad (\text{D.29})$$

777 Now, the right-hand side is a sum of only N_p terms. These operator conditions are clearly sat-
 778 isfied by the identity, and hence, the overlap matrix element in the denominator of Eq. (D.3)
 779 can be antisymmetrised as follows:

$$\mathbb{O}_{\mathbb{A}\mathbb{A}'} \equiv \langle \phi_{\mathbb{A}} | \phi_{\mathbb{A}'} \rangle \rightarrow N_p \langle \phi_{\mathbb{A}} | \mathcal{P}\phi_{\mathbb{A}'} \rangle = N_p \sum_{j=1}^{N_p} s_j \langle \phi_{\mathbb{A}} | \phi_{\tilde{\mathbb{A}}'(j)} \rangle = N_p \sum_{j=1}^{N_p} \frac{s_j (2\pi)^N}{\det[\mathbb{A} + \tilde{\mathbb{A}}'(j)]}. \quad (\text{D.30})$$

780 Equation (D.29) additionally holds for the Hamiltonian \mathcal{H} in Eq. (1), but not for the density
 781 matrices in Appendix C, and thus the numerator of Eq. (D.3) must be antisymmetrised by using
 782 Eq. (D.28). Calculations of structural properties are consequently much longer than those of
 783 energy and excitation spectra. Note that the redefined correlation matrices $\tilde{\mathbb{A}}(i)$ and $\tilde{\mathbb{A}}'(j)$ will
 784 affect the values of the \mathbb{B} matrix, \mathbf{b} vector, and b_1 scalar first appearing in Eq. (D.6) (as well as
 785 their primed equivalents), and all subsequent quantities that depend on these. Equation (D.29)
 786 is very useful since in the ECG method, the principal limiting factor on computational time for
 787 increasing particle number N is the number of permutations N_p required to antisymmetrise
 788 the wave function, as we discussed in Appendix A.

789 E Derivation of the Two-Body Term in the Pair Correlator

790 We can directly extend the approach in Appendix D to derive a closed analytical expression for
 791 the two-body term in Eq. (C.1). To this end, we consider the two-body density matrix for spin-
 792 \uparrow -spin- \downarrow pairs in real space, Eq. (C.10), and we calculate its matrix elements in the explicitly
 793 correlated Gaussian basis. The two-body equivalent of Eq. (D.3) is shown below:

$$\begin{aligned} \frac{[\rho(\mathbf{r}_{\uparrow}, \mathbf{r}'_{\uparrow}; \mathbf{r}_{\downarrow}, \mathbf{r}'_{\downarrow})]_{\mathbb{A}\mathbb{A}'}}{\mathbb{O}_{\mathbb{A}\mathbb{A}'}} &\equiv \frac{\langle \phi_{\mathbb{A}} | \rho | \phi_{\mathbb{A}'} \rangle}{\langle \phi_{\mathbb{A}} | \phi_{\mathbb{A}'} \rangle} \\ &= (\mathbb{O}_{\mathbb{A}\mathbb{A}'})^{-1} \int \dots \int d^{2N-4} \mathbf{y}_{\text{red}} \left[\int \int d^2 \mathbf{r}_1^{\uparrow} d^2 \mathbf{r}_2^{\downarrow} \delta(\mathbf{r}_{\uparrow} - \mathbf{r}_1^{\uparrow}) \delta(\mathbf{r}_{\downarrow} - \mathbf{r}_2^{\downarrow}) \phi_{\mathbb{A}}(\mathbf{x}) \right] \times \\ &\quad \left[\int \int d^2 \mathbf{r}_1^{\uparrow} d^2 \mathbf{r}_2^{\downarrow} \delta(\mathbf{r}'_{\uparrow} - \mathbf{r}_1^{\uparrow}) \delta(\mathbf{r}'_{\downarrow} - \mathbf{r}_2^{\downarrow}) \phi_{\mathbb{A}'}(\mathbf{x}) \right], \end{aligned} \quad (\text{E.1})$$

794 where now $\mathbf{y}_{\text{red}} = (\mathbf{r}_3^{\uparrow}, \mathbf{r}_4^{\downarrow}, \dots, \mathbf{r}_{N-1}^{\uparrow}, \mathbf{r}_N^{\downarrow})$, while $\mathbb{O}_{\mathbb{A}\mathbb{A}'} \equiv \langle \phi_{\mathbb{A}} | \phi_{\mathbb{A}'} \rangle$ is still defined by Eq. (D.4).
 795 By using Eqs. (A.1) and (D.5), we rewrite the basis function $\phi_{\mathbb{A}}$ in terms of \mathbf{y} and separate off
 796 the \mathbf{r}_1^{\uparrow} and $\mathbf{r}_2^{\downarrow}$ dependencies:

$$\phi_{\mathbb{A}}(\mathbf{y}) = g(\mathbf{0}; \mathbb{B}, \mathbf{y}_{\text{red}}) \exp \left[-\frac{1}{2} b_1 (\mathbf{r}_1^{\uparrow})^2 - \frac{1}{2} b_2 (\mathbf{r}_2^{\downarrow})^2 - b_3 (\mathbf{r}_1^{\uparrow})^T \mathbf{r}_2^{\downarrow} - (\mathbf{b}_1^T \mathbf{y}_{\text{red}})^T \mathbf{r}_1^{\uparrow} - (\mathbf{b}_2^T \mathbf{y}_{\text{red}})^T \mathbf{r}_2^{\downarrow} \right]. \quad (\text{E.2})$$

797 Above, the $(N-2) \times (N-2)$ -dimensional matrix \mathbb{B} is given by $\mathbb{U}^T \mathbb{A} \mathbb{U}$ with the first and second
 798 rows and columns removed. Equation (E.2) additionally contains two $(N-2)$ -dimensional vec-
 799 tors:

$$\mathbf{b}_1 = ((\mathbb{U}^T \mathbb{A} \mathbb{U})_{13}, (\mathbb{U}^T \mathbb{A} \mathbb{U})_{14}, \dots, (\mathbb{U}^T \mathbb{A} \mathbb{U})_{1N}), \quad (\text{E.3})$$

$$\mathbf{b}_2 = ((\mathbf{U}^T \mathbb{A} \mathbf{U})_{23}, (\mathbf{U}^T \mathbb{A} \mathbf{U})_{24}, \dots, (\mathbf{U}^T \mathbb{A} \mathbf{U})_{2N}), \quad (\text{E.4})$$

800 and three scalars: $b_1 = (\mathbf{U}^T \mathbb{A} \mathbf{U})_{11}$, $b_2 = (\mathbf{U}^T \mathbb{A} \mathbf{U})_{22}$, $b_3 = (\mathbf{U}^T \mathbb{A} \mathbf{U})_{12}$. To be clear, we mention
801 that

$$(\mathbf{b}_i^T \mathbf{y}_{\text{red}})^T \mathbf{r}_i^\sigma = \sum_{j=3}^N (\mathbf{b}_i)_{j-2} \mathbf{y}_j^T \mathbf{r}_i^\sigma, \quad (\text{E.5})$$

802 where $(\mathbf{b}_i)_j$ denotes the j^{th} element of the vector \mathbf{b}_i (with $i = 1, 2$). We also define analogous
803 quantities $\{\mathbb{B}', \mathbf{b}'_1, \mathbf{b}'_2, b'_1, b'_2, b'_3\}$ which correspond to the basis function $\phi_{\mathbb{A}'}$. To proceed, we
804 substitute the expressions for $\phi_{\mathbb{A}}(\mathbf{x}) \rightarrow \phi_{\mathbb{A}}(\mathbf{y})$ and $\phi_{\mathbb{A}'}(\mathbf{x}) \rightarrow \phi_{\mathbb{A}'}(\mathbf{y})$ into Eq. (E.1), and then
805 evaluate the four Dirac delta functions. This gives

$$\begin{aligned} [\rho(\mathbf{r}_\uparrow, \mathbf{r}'_\uparrow; \mathbf{r}_\downarrow, \mathbf{r}'_\downarrow)]_{\mathbb{A}\mathbb{A}'} &\equiv \langle \phi_{\mathbb{A}} | \rho | \phi_{\mathbb{A}'} \rangle = \int \dots \int d^{2N-4} \mathbf{y}_{\text{red}} g(\mathbf{0}; \mathbb{B}, \mathbf{y}_{\text{red}}) g(\mathbf{0}; \mathbb{B}', \mathbf{y}_{\text{red}}) \times \\ &\exp\left\{-\frac{1}{2} b_1 \mathbf{r}_\uparrow^2 - \frac{1}{2} b_2 \mathbf{r}_\downarrow^2 - b_3 \mathbf{r}_\uparrow^T \mathbf{r}_\downarrow - (\mathbf{b}_1^T \mathbf{y}_{\text{red}})^T \mathbf{r}_\uparrow - (\mathbf{b}_2^T \mathbf{y}_{\text{red}})^T \mathbf{r}_\downarrow\right\} \times \\ &\exp\left\{-\frac{1}{2} b'_1 (\mathbf{r}'_\uparrow)^2 - \frac{1}{2} b'_2 (\mathbf{r}'_\downarrow)^2 - b'_3 (\mathbf{r}'_\uparrow)^T \mathbf{r}'_\downarrow - [(\mathbf{b}'_1)^T \mathbf{y}_{\text{red}}]^T \mathbf{r}'_\uparrow - [(\mathbf{b}'_2)^T \mathbf{y}_{\text{red}}]^T \mathbf{r}'_\downarrow\right\}, \end{aligned} \quad (\text{E.6})$$

806 which can be reformulated as

$$\begin{aligned} [\rho(\mathbf{r}_\uparrow, \mathbf{r}'_\uparrow; \mathbf{r}_\downarrow, \mathbf{r}'_\downarrow)]_{\mathbb{A}\mathbb{A}'} &= \int d^{2N-4} \mathbf{y}_{\text{red}} g[-(\mathbf{b}_1 \mathbf{r}_\uparrow + \mathbf{b}_2 \mathbf{r}_\downarrow + \mathbf{b}'_1 \mathbf{r}'_\uparrow + \mathbf{b}'_2 \mathbf{r}'_\downarrow); \mathbb{B} + \mathbb{B}', \mathbf{y}_{\text{red}}] \times \\ &\exp\left\{-\left[\frac{1}{2} b_1 \mathbf{r}_\uparrow^2 + \frac{1}{2} b_2 \mathbf{r}_\downarrow^2 + b_3 \mathbf{r}_\uparrow^T \mathbf{r}_\downarrow + \frac{1}{2} b'_1 (\mathbf{r}'_\uparrow)^2 + \frac{1}{2} b'_2 (\mathbf{r}'_\downarrow)^2 + b'_3 (\mathbf{r}'_\uparrow)^T \mathbf{r}'_\downarrow\right]\right\}. \end{aligned} \quad (\text{E.7})$$

807 Here $\mathbf{b}_1 \mathbf{r}_\uparrow$, for instance, is an $(N-2)$ -dimensional supervector with elements $(\mathbf{b}_1)_j \mathbf{r}_\uparrow$, where
808 $j = 1, \dots, N-2$. By applying the identity in Eq. (D.10), we can solve the integral over \mathbf{y}_{red} to
809 yield an expression for the ECG matrix elements of the two-body density matrix in real space:

$$\begin{aligned} [\rho(\mathbf{r}_\uparrow, \mathbf{r}'_\uparrow; \mathbf{r}_\downarrow, \mathbf{r}'_\downarrow)]_{\mathbb{A}\mathbb{A}'} &= a_1 \exp\left\{-\frac{1}{2} [c_1 \mathbf{r}_\uparrow^2 + c'_1 (\mathbf{r}'_\uparrow)^2 + c_2 \mathbf{r}_\downarrow^2 + c'_2 (\mathbf{r}'_\downarrow)^2 + d_1 \mathbf{r}_\uparrow^T \mathbf{r}_\downarrow + \right. \\ &\left. d'_1 (\mathbf{r}'_\uparrow)^T \mathbf{r}'_\downarrow - f_1 \mathbf{r}_\uparrow^T \mathbf{r}'_\downarrow - f_2 \mathbf{r}_\downarrow^T \mathbf{r}'_\uparrow - f_3 \mathbf{r}_\uparrow^T \mathbf{r}'_\downarrow - f_4 \mathbf{r}_\downarrow^T \mathbf{r}'_\uparrow]\right\}, \end{aligned} \quad (\text{E.8})$$

810 which depends on the following scalars,

$$a_1 = \frac{(2\pi)^{N-2}}{\det[\mathbb{B} + \mathbb{B}']}, \quad (\text{E.9})$$

$$c_1 = b_1 - \mathbf{b}_1^T \mathbb{C} \mathbf{b}_1, \quad d'_1 = 2b'_3 - (\mathbf{b}'_1)^T \mathbb{C} \mathbf{b}'_2 - (\mathbf{b}'_2)^T \mathbb{C} \mathbf{b}'_1, \quad (\text{E.10})$$

$$c'_1 = b'_1 - (\mathbf{b}'_1)^T \mathbb{C} \mathbf{b}'_1, \quad f_1 = \mathbf{b}_1^T \mathbb{C} \mathbf{b}'_1 + (\mathbf{b}'_1)^T \mathbb{C} \mathbf{b}_1, \quad (\text{E.11})$$

$$c_2 = b_2 - \mathbf{b}_2^T \mathbb{C} \mathbf{b}_2, \quad f_2 = \mathbf{b}_2^T \mathbb{C} \mathbf{b}'_2 + (\mathbf{b}'_2)^T \mathbb{C} \mathbf{b}_2, \quad (\text{E.12})$$

$$c'_2 = b'_2 - (\mathbf{b}'_2)^T \mathbb{C} \mathbf{b}'_2, \quad f_3 = \mathbf{b}_1^T \mathbb{C} \mathbf{b}'_2 + (\mathbf{b}'_2)^T \mathbb{C} \mathbf{b}_1, \quad (\text{E.13})$$

$$d_1 = 2b_3 - \mathbf{b}_1^T \mathbb{C} \mathbf{b}_2 - \mathbf{b}_2^T \mathbb{C} \mathbf{b}_1, \quad f_4 = \mathbf{b}_2^T \mathbb{C} \mathbf{b}'_1 + (\mathbf{b}'_1)^T \mathbb{C} \mathbf{b}_2, \quad (\text{E.14})$$

811 and on the matrix,

$$\mathbb{C} = (\mathbb{B} + \mathbb{B}')^{-1}. \quad (\text{E.15})$$

812 Next, we Fourier transform Eq. (E.8) according to Eq. (C.9) in order to obtain the ECG ma-
813 trix elements of the two-body density matrix in momentum space:

$$[\tilde{\rho}(\mathbf{p}_1, \mathbf{p}_2)]_{\mathbb{A}\mathbb{A}'} = \frac{1}{(2\pi)^4} \int \dots \int d^2 \mathbf{r}_\uparrow d^2 \mathbf{r}'_\uparrow d^2 \mathbf{r}_\downarrow d^2 \mathbf{r}'_\downarrow [\rho(\mathbf{r}_\uparrow, \mathbf{r}'_\uparrow; \mathbf{r}_\downarrow, \mathbf{r}'_\downarrow)]_{\mathbb{A}\mathbb{A}'} e^{-i\mathbf{p}_1 \cdot (\mathbf{r}'_\uparrow - \mathbf{r}_\uparrow)} e^{-i\mathbf{p}_2 \cdot (\mathbf{r}'_\downarrow - \mathbf{r}_\downarrow)}. \quad (\text{E.16})$$

814 By changing variables to $\mathbf{X}_\uparrow = \mathbf{r}'_\uparrow - \mathbf{r}_\uparrow$ and $\mathbf{X}_\downarrow = \mathbf{r}'_\downarrow - \mathbf{r}_\downarrow$, Eq. (E.16) becomes

$$\begin{aligned} [\tilde{\rho}(\mathbf{p}_1, \mathbf{p}_2)]_{\text{AA}'} &= \frac{a_1}{(2\pi)^4} \int \cdots \int d^2\mathbf{r}_\uparrow d^2\mathbf{r}_\downarrow d^2\mathbf{X}_\uparrow d^2\mathbf{X}_\downarrow \exp[-i(p_1^x X_\uparrow^x + p_1^y X_\uparrow^y + p_2^x X_\downarrow^x + p_2^y X_\downarrow^y)] \times \\ &\exp\left(\frac{1}{2} \left\{ g_1 [(r_\uparrow^x)^2 + (r_\uparrow^y)^2] + g_2 [(r_\downarrow^x)^2 + (r_\downarrow^y)^2] + g_3 [r_\uparrow^x r_\downarrow^x + r_\uparrow^y r_\downarrow^y] + \right. \right. \\ &\quad \left. \left. h_{\text{temp}}^{(1,x)} r_\uparrow^x + h_{\text{temp}}^{(1,y)} r_\uparrow^y + h_{\text{temp}}^{(2,x)} r_\downarrow^x + h_{\text{temp}}^{(2,y)} r_\downarrow^y + h_{\text{temp}}^{(3)} \right\} \right), \end{aligned} \quad (\text{E.17})$$

815 where

$$g_1 = f_1 - c_1 - c'_1, \quad (\text{E.18})$$

$$g_2 = f_2 - c_2 - c'_2, \quad (\text{E.19})$$

$$g_3 = f_3 + f_4 - d_1 - d'_1, \quad (\text{E.20})$$

816 are constant scalars, while

$$h_{\text{temp}}^{(1,i)} = (f_1 - 2c'_1)X_\uparrow^i + (f_3 - d'_1)X_\downarrow^i, \quad (\text{E.21})$$

$$h_{\text{temp}}^{(2,i)} = (f_4 - d'_1)X_\uparrow^i + (f_2 - 2c'_2)X_\downarrow^i, \quad (\text{E.22})$$

$$h_{\text{temp}}^{(3)} = -c'_1[(X_\uparrow^x)^2 + (X_\uparrow^y)^2] - c'_2[(X_\downarrow^x)^2 + (X_\downarrow^y)^2] - d'_1(X_\uparrow^x X_\downarrow^x + X_\uparrow^y X_\downarrow^y), \quad (\text{E.23})$$

817 are temporary functions of the integration variables \mathbf{X}_\uparrow and \mathbf{X}_\downarrow (with $i = x, y$). In similarity to
818 the previous section, the integral over \mathbf{r}_\downarrow can be performed analytically for $g_2 < 0$, and then
819 so can the integral over \mathbf{r}_\uparrow for $4g_1g_2 - g_3^2 > 0$:

$$\begin{aligned} &\int_{-\infty}^{+\infty} \cdots \int_{-\infty}^{+\infty} dr_\uparrow^x dr_\uparrow^y dr_\downarrow^x dr_\downarrow^y \exp\left(\frac{1}{2} \left\{ g_1 [(r_\uparrow^x)^2 + (r_\uparrow^y)^2] + g_2 [(r_\downarrow^x)^2 + (r_\downarrow^y)^2] + \right. \right. \\ &\quad \left. \left. g_3 [r_\uparrow^x r_\downarrow^x + r_\uparrow^y r_\downarrow^y] + h_{\text{temp}}^{(1,x)} r_\uparrow^x + h_{\text{temp}}^{(1,y)} r_\uparrow^y + h_{\text{temp}}^{(2,x)} r_\downarrow^x + h_{\text{temp}}^{(2,y)} r_\downarrow^y \right\} \right) \\ &= \frac{16\pi^2}{4g_1g_2 - g_3^2} \exp\left[-\frac{1/2}{4g_1g_2 - g_3^2} \times \right. \\ &\quad \left. \left(g_1 \left\{ [h_{\text{temp}}^{(2,x)}]^2 + [h_{\text{temp}}^{(2,y)}]^2 \right\} + g_2 \left\{ [h_{\text{temp}}^{(1,x)}]^2 + [h_{\text{temp}}^{(1,y)}]^2 \right\} - g_3 \left\{ h_{\text{temp}}^{(1,x)} h_{\text{temp}}^{(2,x)} + h_{\text{temp}}^{(1,y)} h_{\text{temp}}^{(2,y)} \right\} \right) \right] \\ &= \frac{16\pi^2}{t_0} \exp\left(\frac{1}{2t_0} \left\{ t_1 [(X_\uparrow^x)^2 + (X_\uparrow^y)^2] + t_2 [(X_\downarrow^x)^2 + (X_\downarrow^y)^2] + t_3 [X_\uparrow^x X_\downarrow^x + X_\uparrow^y X_\downarrow^y] \right\} \right), \end{aligned} \quad (\text{E.24})$$

820 where we have defined

$$t_0 = 4g_1g_2 - g_3^2, \quad (\text{E.25})$$

$$t_1 = -(f_4 - d'_1)^2 g_1 - (f_1 - 2c'_1)^2 g_2 + (f_4 - d'_1)(f_1 - 2c'_1) g_3, \quad (\text{E.26})$$

$$t_2 = -(f_2 - 2c'_2)^2 g_1 - (f_3 - d'_1)^2 g_2 + (f_3 - d'_1)(f_2 - 2c'_2) g_3, \quad (\text{E.27})$$

$$\begin{aligned} t_3 &= -2(f_4 - d'_1)(f_2 - 2c'_2) g_1 - 2(f_3 - d'_1)(f_1 - 2c'_1) g_2 \\ &\quad + [(f_4 - d'_1)(f_3 - d'_1) + (f_2 - 2c'_2)(f_1 - 2c'_1)] g_3. \end{aligned} \quad (\text{E.28})$$

821 Therefore, Eq. (E.17) can now be written as

$$\begin{aligned} [\tilde{\rho}(\mathbf{p}_1, \mathbf{p}_2)]_{\text{AA}'} &= \frac{a_1}{(2\pi)^4} \frac{16\pi^2}{t_0} \iint d^2\mathbf{X}_\uparrow d^2\mathbf{X}_\downarrow \exp[-i(p_1^x X_\uparrow^x + p_1^y X_\uparrow^y + p_2^x X_\downarrow^x + p_2^y X_\downarrow^y)] \times \\ &\exp\left(\frac{1}{2} \left\{ s_1 [(X_\uparrow^x)^2 + (X_\uparrow^y)^2] + s_2 [(X_\downarrow^x)^2 + (X_\downarrow^y)^2] + s_3 [X_\uparrow^x X_\downarrow^x + X_\uparrow^y X_\downarrow^y] \right\} \right), \end{aligned} \quad (\text{E.29})$$

822 which involves

$$s_1 = t_1/t_0 - c'_1, \quad (\text{E.30})$$

$$s_2 = t_2/t_0 - c'_2, \quad (\text{E.31})$$

$$s_3 = t_3/t_0 - d'_1. \quad (\text{E.32})$$

823 At this point, the integral over \mathbf{X}_\downarrow can be carried out analytically for $s_2 < 0$:

$$\begin{aligned} & \int_{-\infty}^{+\infty} \int_{-\infty}^{+\infty} dX_\downarrow^x dX_\downarrow^y \exp[-i(p_2^x X_\downarrow^x + p_2^y X_\downarrow^y)] \times \\ & \exp\left(\frac{1}{2} \left\{ s_2 [(X_\downarrow^x)^2 + (X_\downarrow^y)^2] + s_3 [X_\uparrow^x X_\downarrow^x + X_\uparrow^y X_\downarrow^y] \right\}\right) \\ & = -\frac{2\pi}{s_2} \exp\left(\frac{1}{8s_2} \left\{ 4[(p_2^x)^2 + (p_2^y)^2] - s_3^2 [(X_\uparrow^x)^2 + (X_\uparrow^y)^2] + 4is_3 (p_2^x X_\uparrow^x + p_2^y X_\uparrow^y) \right\}\right). \end{aligned} \quad (\text{E.33})$$

824 Subsequently, for $4s_1s_2 - s_3^2 > 0$ we can analytically evaluate the integral over \mathbf{X}_\uparrow as well:

$$\begin{aligned} & \int_{-\infty}^{+\infty} \int_{-\infty}^{+\infty} dX_\uparrow^x dX_\uparrow^y \exp[-i(p_1^x X_\uparrow^x + p_1^y X_\uparrow^y)] \times \exp\left\{\frac{1}{2} s_1 [(X_\uparrow^x)^2 + (X_\uparrow^y)^2]\right\} \times \\ & \exp\left(\frac{1}{8s_2} \left\{ 4[(p_2^x)^2 + (p_2^y)^2] - s_3^2 [(X_\uparrow^x)^2 + (X_\uparrow^y)^2] + 4is_3 (p_2^x X_\uparrow^x + p_2^y X_\uparrow^y) \right\}\right) \\ & = -\frac{8\pi s_2}{4s_1s_2 - s_3^2} \exp\left(\frac{2}{4s_1s_2 - s_3^2} \left\{ s_2 [(p_1^x)^2 + (p_1^y)^2] + s_1 [(p_2^x)^2 + (p_2^y)^2] - s_3 (p_1^x p_2^x + p_1^y p_2^y) \right\}\right). \end{aligned} \quad (\text{E.34})$$

825 Collating and simplifying these results leads to a compact expression for the ECG matrix ele-
826 ments of the momentum-space two-body density matrix for spin- \uparrow -spin- \downarrow pairs:

$$\begin{aligned} [\tilde{\rho}(\mathbf{p}_1, \mathbf{p}_2)]_{\mathbb{A}\mathbb{A}'} &= \frac{a_1}{(2\pi)^4} \frac{16\pi^2}{4g_1g_2 - g_3^2} \left(-\frac{2\pi}{s_2}\right) \left(-\frac{8\pi s_2}{4s_1s_2 - s_3^2}\right) \times \\ & \exp\left(\frac{2}{4s_1s_2 - s_3^2} \left\{ s_2 [(p_1^x)^2 + (p_1^y)^2] + s_1 [(p_2^x)^2 + (p_2^y)^2] - s_3 (p_1^x p_2^x + p_1^y p_2^y) \right\}\right) \\ & = \frac{16a_1}{(4g_1g_2 - g_3^2)(4s_1s_2 - s_3^2)} \exp\left\{\frac{2}{4s_1s_2 - s_3^2} \left[s_2 p_1^2 + s_1 p_2^2 - s_3 (p_1^x p_2^x + p_1^y p_2^y) \right]\right\}, \end{aligned} \quad (\text{E.35})$$

827 with momenta $p_1 \equiv |\mathbf{p}_1|$ and $p_2 \equiv |\mathbf{p}_2|$. We have checked numerically that g_2 and s_2 are less
828 than zero, while $4g_1g_2 - g_3^2$ and $4s_1s_2 - s_3^2$ are greater than zero, as required. The expectation
829 value $\langle n_\uparrow(\mathbf{p}_1)n_\downarrow(\mathbf{p}_2) \rangle$ can now be evaluated with respect to the ground state in a manner akin
830 to Eq. (D.25). For particles with both opposite spins and opposite momenta ($\mathbf{p}_1 = -\mathbf{p}_2 \equiv \mathbf{p}$)
831 this final result simplifies even further [and notice its similarity to Eq. (D.24)]:

$$[\tilde{\rho}(\mathbf{p}, -\mathbf{p})]_{\mathbb{A}\mathbb{A}'} = \frac{16a_1}{(4g_1g_2 - g_3^2)(4s_1s_2 - s_3^2)} \exp\left[\frac{2(s_1 + s_2 + s_3)}{4s_1s_2 - s_3^2} p^2\right], \quad (\text{E.36})$$

832 with momentum $p \equiv |\mathbf{p}|$. We remark that for clarity, we have used the unsymmetrised basis
833 functions defined by Eq. (D.2) in the above discussion. However, in actuality, these must be
834 antisymmetrised according to the prescription provided at the end of the previous appendix.

835 F Bardeen–Cooper–Schrieffer (BCS) Theory

836 In this appendix, we describe the BCS theoretical treatment for completeness and ease of ac-
837 cess. The ensuing derivation of the opposite-momentum pair correlation function, $\mathcal{C}^{(2)}(\mathbf{p}, -\mathbf{p})$
838 $\equiv \mathcal{C}^{(2)}(p)$, was first performed in Ref. [24] and the results are relevant to Figs. 4 and 6 in the
839 current work.

840 Within BCS theory, the expectation values in Eqs. (C.2)–(C.4) can be directly evaluated
841 with respect to the ground state by applying the Bogoliubov transformation:

$$c_{\mathbf{p}\uparrow} = u_p \gamma_{\mathbf{p}\uparrow} - v_p \gamma_{-\mathbf{p}\downarrow}^\dagger, \quad (\text{F1})$$

$$c_{\mathbf{p}\downarrow} = u_p \gamma_{\mathbf{p}\downarrow} + v_p \gamma_{-\mathbf{p}\uparrow}^\dagger, \quad (\text{F2})$$

842 where

$$u_p^2 = (1 + \varepsilon_p / \xi_p) / 2, \quad (\text{F3})$$

$$v_p^2 = (1 - \varepsilon_p / \xi_p) / 2. \quad (\text{F4})$$

843 The BCS spectrum of excitations is given by $\xi_p = (\varepsilon_p^2 + \Delta^2)^{1/2}$. Here, $\varepsilon_p = p^2 / (2m) - \varepsilon_F$ is
844 the free electron dispersion measured relative to the Fermi energy, and the mean-field value of
845 the superfluid gap is $\Delta = (2\varepsilon_b \varepsilon_F)^{1/2}$ [12]. By replacing the particle creation and annihilation
846 operators ($c_{\mathbf{p}\sigma}^\dagger, c_{\mathbf{p}\sigma}$) with fermionic quasiparticle operators ($\gamma_{\mathbf{p}\sigma}^\dagger, \gamma_{\mathbf{p}\sigma}$), and then using the fact
847 that the BCS ground state is the quasiparticle vacuum, $\gamma_{\mathbf{p}\sigma} |\Psi_{\text{BCS}}\rangle = 0$, we arrive at

$$\begin{aligned} \mathcal{C}^{(2)}(p) &= \langle c_{\mathbf{p}\uparrow}^\dagger c_{\mathbf{p}\uparrow} c_{-\mathbf{p}\downarrow}^\dagger c_{-\mathbf{p}\downarrow} \rangle - \langle c_{\mathbf{p}\uparrow}^\dagger c_{\mathbf{p}\uparrow} \rangle \langle c_{-\mathbf{p}\downarrow}^\dagger c_{-\mathbf{p}\downarrow} \rangle \\ &= \mathcal{N}^2 \frac{\Delta^2}{4(\varepsilon_p^2 + \Delta^2)}. \end{aligned} \quad (\text{F5})$$

848 The normalisation factor \mathcal{N} is determined by fixing the single-spin atom number in the non-
849 interacting limit ($\Delta = 0$):

$$N_\uparrow = \int \langle c_{\mathbf{p}\uparrow}^\dagger c_{\mathbf{p}\uparrow} \rangle d\mathbf{p} = 2\pi \mathcal{N} \int_0^\infty v_p^2 p dp. \quad (\text{F6})$$

850 References

- 851 [1] I. Bloch, *Ultracold quantum gases in optical lattices*, Nature **1**, 23–30 (2005),
852 doi:[10.1038/nphys138](https://doi.org/10.1038/nphys138).
- 853 [2] I. Bloch, J. Dalibard and W. Zwerger, *Many-body physics with ultracold gases*, Reviews of
854 Modern Physics **80**, 885–964 (2008), doi:[10.1103/RevModPhys.80.885](https://doi.org/10.1103/RevModPhys.80.885).
- 855 [3] C. Chin, R. Grimm, P. Julienne and E. Tiesinga, *Feshbach resonances in ultracold gases*,
856 Reviews of Modern Physics **82**, 1225–1286 (2010), doi:[10.1103/RevModPhys.82.1225](https://doi.org/10.1103/RevModPhys.82.1225).
- 857 [4] M. Greiner, C. A. Regal and D. S. Jin, *Emergence of a molecular Bose–Einstein condensate*
858 *from a Fermi gas*, Nature **426**, 537–540 (2003), doi:[10.1038/nature02199](https://doi.org/10.1038/nature02199).
- 859 [5] S. Jochim, M. Bartenstein, A. Altmeyer, G. Hendl, S. Riedl, C. Chin, J. H. Denschlag and
860 R. Grimm, *Bose–Einstein condensation of molecules*, Science **302**, 2101–2103 (2003),
861 doi:[10.1126/science.1093280](https://doi.org/10.1126/science.1093280).

- 862 [6] T. Bourdel, L. Khaykovich, J. Cubizolles, J. Zhang, F. Chevy, M. Teichmann, L. Tarruell,
863 S. J. J. M. F. Kokkelmans and C. Salomon, *Experimental study of the BEC–BCS crossover*
864 *region in lithium 6*, Physical Review Letters **93**, 050401 (2004),
865 doi:[10.1103/PhysRevLett.93.050401](https://doi.org/10.1103/PhysRevLett.93.050401).
- 866 [7] J. Kinast, A. Turlapov, J. E. Thomas, Q. Chen, J. Stajic and K. Levin, *Heat capacity of a*
867 *strongly interacting Fermi gas*, Science **307**, 1296–1299 (2005),
868 doi:[10.1126/science.1109220](https://doi.org/10.1126/science.1109220).
- 869 [8] M. W. Zwierlein, J. R. Abo-Shaeer, A. Schirotzek, C. H. Schunck and W. Ketterle,
870 *Vortices and superfluidity in a strongly interacting Fermi gas*, Nature **435**, 1047–1051
871 (2005), doi:[10.1038/nature03858](https://doi.org/10.1038/nature03858).
- 872 [9] G. B. Partridge, K. E. Strecker, R. I. Kamar, M. W. Jack and R. G. Hulet, *Molecular probe*
873 *of pairing in the BEC–BCS crossover*, Physical Review Letters **95**, 020404 (2005),
874 doi:[10.1103/PhysRevLett.95.020404](https://doi.org/10.1103/PhysRevLett.95.020404).
- 875 [10] S. Giorgini, L. P. Pitaevskii and S. Stringari, *Theory of ultracold atomic fermi gases*,
876 Reviews of Modern Physics **80**, 1215–1274 (2008), doi:[10.1103/RevModPhys.80.1215](https://doi.org/10.1103/RevModPhys.80.1215).
- 877 [11] W. Zwerger, ed., *Lecture Notes in Physics (vol. 836): The BCS–BEC Crossover and the*
878 *Unitary Fermi Gas*, Springer–Verlag Publishing (2012).
- 879 [12] M. Randeria, J.-M. Duan and L.-Y. Shieh, *Bound states, Cooper pairing, and Bose*
880 *condensation in two dimensions*, Physical Review Letters **62**, 981–984 (1989),
881 doi:[10.1103/PhysRevLett.62.981](https://doi.org/10.1103/PhysRevLett.62.981).
- 882 [13] M. Randeria, J.-M. Duan and L.-Y. Shieh, *Superconductivity in a two-dimensional Fermi*
883 *gas: Evolution from Cooper pairing to Bose condensation*, Physical Review B **41**, 327–343
884 (1990), doi:[10.1103/PhysRevB.41.327](https://doi.org/10.1103/PhysRevB.41.327).
- 885 [14] D. S. Petrov and G. V. Shlyapnikov, *Interatomic collisions in a tightly confined Bose gas*,
886 Physical Review A **64**, 012706 (2001), doi:[10.1103/PhysRevA.64.012706](https://doi.org/10.1103/PhysRevA.64.012706).
- 887 [15] D. S. Petrov, M. A. Baranov and G. V. Shlyapnikov, *Superfluid transition in*
888 *quasi-two-dimensional Fermi gases*, Physical Review A **67**, 031601 (2003),
889 doi:[10.1103/PhysRevA.67.031601](https://doi.org/10.1103/PhysRevA.67.031601).
- 890 [16] S. S. Botelho and C. A. R. Sá de Melo, *Vortex-antivortex lattice in ultracold fermionic*
891 *gases*, Physical Review Letters **96**, 040404 (2006),
892 doi:[10.1103/PhysRevLett.96.040404](https://doi.org/10.1103/PhysRevLett.96.040404).
- 893 [17] L. Salasnich, *Condensate fraction of a two-dimensional attractive Fermi gas*, Physical
894 Review A **76**, 015601 (2007), doi:[10.1103/PhysRevA.76.015601](https://doi.org/10.1103/PhysRevA.76.015601).
- 895 [18] W. Zhang, G.-D. Lin and L.-M. Duan, *BCS–BEC crossover of a quasi-two-dimensional*
896 *Fermi gas: The significance of dressed molecules*, Physical Review A **77**, 063613 (2008),
897 doi:[10.1103/PhysRevA.77.063613](https://doi.org/10.1103/PhysRevA.77.063613).
- 898 [19] W. Zhang, G.-D. Lin and L.-M. Duan, *Berezinskii–Kosterlitz–Thouless transition in a*
899 *trapped quasi-two-dimensional Fermi gas near a Feshbach resonance*, Physical Review A
900 **78**, 043617 (2008), doi:[10.1103/PhysRevA.78.043617](https://doi.org/10.1103/PhysRevA.78.043617).
- 901 [20] M. Iskin and C. A. R. Sá de Melo, *Evolution from BCS to Berezinskii–Kosterlitz–Thouless*
902 *superfluidity in one-dimensional optical lattices*, Physical Review Letters **103**, 165301
903 (2009), doi:[10.1103/PhysRevLett.103.165301](https://doi.org/10.1103/PhysRevLett.103.165301).

- 904 [21] E. J. Mueller, *Review of pseudogaps in strongly interacting Fermi gases*, Reports on
905 Progress in Physics **80**, 104401 (2017), doi:[10.1088/1361-6633/aa7e53](https://doi.org/10.1088/1361-6633/aa7e53).
- 906 [22] P. A. Murthy, M. Neidig, R. Klemt, L. Bayha, I. Boettcher, T. Enss, M. Holten, G. Zürn,
907 P. M. Preiss and S. Jochim, *High-temperature pairing in a strongly interacting*
908 *two-dimensional Fermi gas*, Science **359**, 452 (2018), doi:[10.1126/science.aan5950](https://doi.org/10.1126/science.aan5950).
- 909 [23] L. Bayha, M. Holten, R. Klemt, K. Subramanian, J. Bjerlin, S. M. Reimann, G. M. Bruun,
910 P. M. Preiss and S. Jochim, *Observing the emergence of a quantum phase transition shell*
911 *by shell*, Nature **587**, 583–587 (2020), doi:[10.1038/s41586-020-2936-y](https://doi.org/10.1038/s41586-020-2936-y).
- 912 [24] M. Holten, L. Bayha, K. Subramanian, S. Brandstetter, C. Heintze, P. Lunt, P. M. Preiss
913 and S. Jochim, *Observation of Cooper pairs in a mesoscopic two-dimensional Fermi gas*,
914 Nature **606**, 287–291 (2022), doi:[10.1038/s41586-022-04678-1](https://doi.org/10.1038/s41586-022-04678-1).
- 915 [25] G. M. Bruun, *Long-lived Higgs mode in a two-dimensional confined Fermi system*,
916 Physical Review A **90**, 023621 (2014), doi:[10.1103/PhysRevA.90.023621](https://doi.org/10.1103/PhysRevA.90.023621).
- 917 [26] J. Bjerlin, S. M. Reimann and G. M. Bruun, *Few-body precursor of the Higgs mode in a*
918 *Fermi gas*, Physical Review Letters **116**, 155302 (2016),
919 doi:[10.1103/PhysRevLett.116.155302](https://doi.org/10.1103/PhysRevLett.116.155302).
- 920 [27] C. Bradly, *Few-body physics of strongly interacting trapped quantum gases*, Ph.D. Thesis,
921 University of Melbourne (2016).
- 922 [28] F. Resare and J. Hofmann, *Few-to-many particle crossover of pair excitations in a*
923 *superfluid*, arXiv: 2208.03762 (v1), pp. 1–6 (2022), doi:[10.48550/arXiv.2208.03762](https://doi.org/10.48550/arXiv.2208.03762).
- 924 [29] R. Richardson, *A restricted class of exact eigenstates of the pairing-force Hamiltonian*,
925 Physics Letters **3**, 277–279 (1963), doi:[10.1016/0031-9163\(63\)90259-2](https://doi.org/10.1016/0031-9163(63)90259-2).
- 926 [30] R. Richardson and N. Sherman, *Exact eigenstates of the pairing-force Hamiltonian*,
927 Nuclear Physics **52**, 221–238 (1964), doi:[10.1016/0029-5582\(64\)90687-X](https://doi.org/10.1016/0029-5582(64)90687-X).
- 928 [31] J. von Delft and F. Braun, *Superconductivity in Ultrasmall Grains: Introduction to*
929 *Richardson’s Exact Solution* — in “Quantum Mesoscopic Phenomena and Mesoscopic
930 *Devices in Microelectronics*”, chap. 24, pp. 361–370, Kluwer Academic Publishers,
931 doi:[10.1007/978-94-011-4327-1_24](https://doi.org/10.1007/978-94-011-4327-1_24) (2000).
- 932 [32] K. Varga and Y. Suzuki, *Precise solution of few-body problems with the stochastic*
933 *variational method on a correlated Gaussian basis*, Physical Review C **52**, 2885–2905
934 (1995), doi:[10.1103/PhysRevC.52.2885](https://doi.org/10.1103/PhysRevC.52.2885).
- 935 [33] K. Varga and Y. Suzuki, *Stochastic variational method with a correlated Gaussian basis*,
936 Physical Review A **53**, 1907–1910 (1996), doi:[10.1103/PhysRevA.53.1907](https://doi.org/10.1103/PhysRevA.53.1907).
- 937 [34] S. F. Boys, *The integral formulae for the variational solution of the molecular*
938 *many-electron wave equation in terms of Gaussian functions with direct electronic*
939 *correlation*, Proceedings of the Royal Society of London A **258**, 402–411 (1960),
940 doi:[10.1098/rspa.1960.0195](https://doi.org/10.1098/rspa.1960.0195).
- 941 [35] K. Singer, *The use of Gaussian (exponential quadratic) wave functions in molecular*
942 *problems — I. General formulae for the evaluation of integrals*, Proceedings of the Royal
943 Society of London A **258**, 412–420 (1960), doi:[10.1098/rspa.1960.0196](https://doi.org/10.1098/rspa.1960.0196).

- 944 [36] J. Mitroy, S. Bubin, W. Horiuchi, Y. Suzuki, L. Adamowicz, W. Cencek, K. Szalewicz,
945 J. Komasa, D. Blume and K. Varga, *Theory and application of explicitly correlated*
946 *Gaussians*, *Reviews of Modern Physics* **85**, 693–749 (2013),
947 doi:[10.1103/RevModPhys.85.693](https://doi.org/10.1103/RevModPhys.85.693).
- 948 [37] K. M. Daily, *Harmonically trapped cold atom systems: Few-body dynamics and application*
949 *to many-body thermodynamics*, Ph.D. Thesis, Washington State University (2012).
- 950 [38] X. Yin, *Universal and non-universal properties of ultracold few-atom systems*, Ph.D.
951 Thesis, Washington State University (2015).
- 952 [39] D. Blume and K. Daily, *Trapped two-component Fermi gases with up to six particles:*
953 *Energetics, structural properties, and molecular condensate fraction*, *Comptes Rendus*
954 *Physique* **12**, 86–109 (2011), doi:[10.1016/j.crhy.2010.11.010](https://doi.org/10.1016/j.crhy.2010.11.010).
- 955 [40] C. J. Bradly, B. C. Mulkerin, A. M. Martin and H. M. Quiney, *Coupled-pair approach for*
956 *strongly interacting trapped fermionic atoms*, *Physical Review A* **90**, 023626 (2014),
957 doi:[10.1103/PhysRevA.90.023626](https://doi.org/10.1103/PhysRevA.90.023626).
- 958 [41] X. Y. Yin and D. Blume, *Trapped unitary two-component Fermi gases with up to ten*
959 *particles*, *Physical Review A* **92**, 013608 (2015), doi:[10.1103/PhysRevA.92.013608](https://doi.org/10.1103/PhysRevA.92.013608).
- 960 [42] J. Levinsen and M. M. Parish, *Bound states in a quasi-two-dimensional Fermi gas*,
961 *Physical Review Letters* **110**, 055304 (2013), doi:[10.1103/PhysRevLett.110.055304](https://doi.org/10.1103/PhysRevLett.110.055304).
- 962 [43] T. Kirk and M. M. Parish, *Three-body correlations in a two-dimensional SU(3) Fermi gas*,
963 *Physical Review A* **96**, 053614 (2017), doi:[10.1103/PhysRevA.96.053614](https://doi.org/10.1103/PhysRevA.96.053614).
- 964 [44] H. Hu, B. C. Mulkerin, U. Toniolo, L. He and X.-J. Liu, *Reduced quantum anomaly in a*
965 *quasi-two-dimensional Fermi superfluid: Significance of the confinement-induced effective*
966 *range of interactions*, *Physical Review Letters* **122**, 070401 (2019),
967 doi:[10.1103/PhysRevLett.122.070401](https://doi.org/10.1103/PhysRevLett.122.070401).
- 968 [45] X. Y. Yin, H. Hu and X.-J. Liu, *Few-body perspective of a quantum anomaly in*
969 *two-dimensional Fermi gases*, *Physical Review Letters* **124**, 013401 (2020),
970 doi:[10.1103/PhysRevLett.124.013401](https://doi.org/10.1103/PhysRevLett.124.013401).
- 971 [46] M. Holten, *From Pauli blocking to Cooper pairs: Emergence in a mesoscopic 2D Fermi gas*,
972 Ph.D. Thesis, Heidelberg University (2022).
- 973 [47] D. M. Stamper-Kurn, H.-J. Miesner, A. P. Chikkatur, S. Inouye, J. Stenger and
974 W. Ketterle, *Reversible formation of a Bose–Einstein condensate*, *Physical Review Letters*
975 **81**, 2194–2197 (1998), doi:[10.1103/PhysRevLett.81.2194](https://doi.org/10.1103/PhysRevLett.81.2194).
- 976 [48] J. J. Sakurai and J. Napolitano, *Modern Quantum Mechanics*, Addison–Wesley
977 Publishing, 2nd edn. (2010).
- 978 [49] B. J. Verhaar, J. P. H. W. van den Eijnde, M. A. J. Voermans and M. M. J. Schaffrath,
979 *Scattering length and effective range in two dimensions: Application to adsorbed hydrogen*
980 *atoms*, *Journal of Physics A: Mathematical and General* **17**, 595–598 (1984),
981 doi:[10.1088/0305-4470/17/3/020](https://doi.org/10.1088/0305-4470/17/3/020).
- 982 [50] S. K. Adhikari, *Quantum scattering in two dimensions*, *American Journal of Physics* **54**,
983 362–367 (1986), doi:[10.1119/1.14623](https://doi.org/10.1119/1.14623).

- 984 [51] S. K. Adhikari, W. G. Gibson and T. K. Lim, *Effective-range theory in two dimensions*,
985 *Journal of Chemical Physics* **85**, 5580–5583 (1986), doi:[10.1063/1.451572](https://doi.org/10.1063/1.451572).
- 986 [52] J. Levinsen and M. M. Parish, *Chapter 1: Strongly interacting two-dimensional Fermi*
987 *gases*, *Annual Review of Cold Atoms and Molecules* **3**, 1–75 (2015),
988 doi:[10.1142/9789814667746_0001](https://doi.org/10.1142/9789814667746_0001).
- 989 [53] E. Braaten and H.-W. Hammer, *Universality in few-body systems with large scattering*
990 *length*, *Physics Reports* **428**, 259–390 (2006), doi:[10.1016/j.physrep.2006.03.001](https://doi.org/10.1016/j.physrep.2006.03.001).
- 991 [54] T. Sowiński, *Few-body perspective on fermionic pairing in one spatial dimension*,
992 *Europhysics Letters* **134**, 33001 (2021), doi:[10.1209/0295-5075/ac0f0e](https://doi.org/10.1209/0295-5075/ac0f0e).
- 993 [55] J. Levinsen, P. Massignan, S. Endo and M. M. Parish, *Universality of the unitary Fermi*
994 *gas: A few-body perspective*, *Journal of Physics B: Atomic, Molecular and Optical Physics*
995 **50**, 072001 (2017), doi:[10.1088/1361-6455/aa5a1e](https://doi.org/10.1088/1361-6455/aa5a1e).
- 996 [56] C. De Boor, *A Practical Guide to Splines*, Springer-Verlag Publishing (1978).
- 997 [57] H. Bachau, E. Cormier, P. Decleva, J. E. Hansen and F. Martín, *Applications of B-splines*
998 *in atomic and molecular physics*, *Reports on Progress in Physics* **64**, 1815–1942 (2001),
999 doi:[10.1088/0034-4885/64/12/205](https://doi.org/10.1088/0034-4885/64/12/205).
- 1000 [58] W. Ketterle and M. W. Zwierlein, *Making, probing and understanding ultracold Fermi*
1001 *gases*, *La Rivista del Nuovo Cimento* **5–6**, 247–422 (2008),
1002 doi:[10.1393/ncr/i2008-10033-1](https://doi.org/10.1393/ncr/i2008-10033-1).
- 1003 [59] J. Bardeen, L. N. Cooper and J. R. Schrieffer, *Theory of superconductivity*, *Physical*
1004 *Review* **108**, 1175–1204 (1957), doi:[10.1103/PhysRev.108.1175](https://doi.org/10.1103/PhysRev.108.1175).
- 1005 [60] M. M. Parish, *The BCS–BEC Crossover — in “Quantum Gas Experiments: Exploring*
1006 *Many-Body States”*, chap. 9, pp. 179–197, Imperial College Press,
1007 doi:[10.1142/9781783264766_0009](https://doi.org/10.1142/9781783264766_0009) (2014).
- 1008 [61] H. Shi, S. Chiesa and S. Zhang, *Ground-state properties of strongly interacting Fermi*
1009 *gases in two dimensions*, *Physical Review A* **92**, 033603 (2015),
1010 doi:[10.1103/PhysRevA.92.033603](https://doi.org/10.1103/PhysRevA.92.033603).
- 1011 [62] Y.-Y. He, H. Shi and S. Zhang, *Precision many-body study of the*
1012 *Berezinskii–Kosterlitz–Thouless transition and temperature-dependent properties in the*
1013 *two-dimensional Fermi gas*, *Physical Review Letters* **129**, 076403 (2022),
1014 doi:[10.1103/PhysRevLett.129.076403](https://doi.org/10.1103/PhysRevLett.129.076403).
- 1015 [63] H. Moriya, H. Tajima, W. Horiuchi, K. Iida and E. Nakano, *Binding two and three α*
1016 *particles in cold neutron matter*, *Physical Review C* **104**, 065801 (2021),
1017 doi:[10.1103/PhysRevC.104.065801](https://doi.org/10.1103/PhysRevC.104.065801).
- 1018 [64] P. Dyke, A. Hogan, I. Herrera, C. C. N. Kuhn, S. Hoinka and C. J. Vale, *Dynamics of a*
1019 *Fermi gas quenched to unitarity*, *Physical Review Letters* **127**, 100405 (2021),
1020 doi:[10.1103/PhysRevLett.127.100405](https://doi.org/10.1103/PhysRevLett.127.100405).
- 1021 [65] J. von Stecher and C. H. Greene, *Spectrum and dynamics of the BCS–BEC crossover from*
1022 *a few-body perspective*, *Physical Review Letters* **99**, 090402 (2007),
1023 doi:[10.1103/PhysRevLett.99.090402](https://doi.org/10.1103/PhysRevLett.99.090402).

- 1024 [66] J. von Stecher, C. H. Greene and D. Blume, *Energetics and structural properties of*
1025 *trapped two-component Fermi gases*, Physical Review A **77**, 043619 (2008),
1026 doi:[10.1103/PhysRevA.77.043619](https://doi.org/10.1103/PhysRevA.77.043619).
- 1027 [67] K. M. Daily and D. Blume, *Energy spectrum of harmonically trapped two-component*
1028 *Fermi gases: Three- and four-particle problem*, Physical Review A **81**, 053615 (2010),
1029 doi:[10.1103/PhysRevA.81.053615](https://doi.org/10.1103/PhysRevA.81.053615).
- 1030 [68] Y. Suzuki and K. Varga, *Stochastic Variational Approach to Quantum Mechanical*
1031 *Few-Body Problems*, Springer–Verlag Publishing (1998).
- 1032 [69] M. Rontani, J. R. Armstrong, Y. Yu, S. Aberg and S. M. Reimann, *Cold fermionic atoms*
1033 *in two-dimensional traps: Pairing versus Hund’s rule*, Physical Review Letters **102**,
1034 060401 (2009), doi:[10.1103/PhysRevLett.102.060401](https://doi.org/10.1103/PhysRevLett.102.060401).
- 1035 [70] M. Rontani, G. Eriksson, S. Aberg and S. M. Reimann, *On the renormalization of contact*
1036 *interactions for the configuration-interaction method in two-dimensions*, Journal of
1037 Physics B: Atomic, Molecular and Optical Physics **50**, 065301 (2017),
1038 doi:[10.1088/1361-6455/aa606a](https://doi.org/10.1088/1361-6455/aa606a).